USING SPECTRAL VEGETATION INDICES TO MEASURE GROSS PRIMARY PRODUCTIVITY AS AN INDICATOR OF LAND DEGRADATION

GEF-LAND DEGRADATION MONITORING PROJECT | REPORT ONE

CONSERVATION INTERNATIONAL

gef
GLOBAL ENVIRONMENT FACILITY
INVESTING IN OUR PLANET

LUND UNIVERSITY

NASA

Using spectral vegetation indices to measure gross primary productivity as an indicator of land degradation

GEF-Land Degradation Monitoring Project
Report One

Compton Tucker[1], Jorge Pinzon[1]

[1]NASA/Goddard Space Flight Center

Mail Code: 610.9

Greenbelt, MD 20771

This report was produced as an output of the Global Environment Facility (GEF)-funded project "Enabling the use of global data sources to assess and monitor land degradation at multiple scales". The project aims to provide guidance on robust methods and a toolbox for assessing and monitoring status of land degradation using remote sensing technology.

For additional information on the project see http://vitalsigns.org/gef-ldmp.

The Land Degradation Monitoring Project is a collaboration of Conservation International, the National Aeronautics and Space Administration (NASA), and Lund University.

SUMMARY

This report is a product of the Global Environment Facility (GEF)-funded project "Enabling the use of global data sources to assess and monitor land degradation at multiple scales". The objective of this project is to provide guidance, methods, and a toolbox to support assessing and monitoring the status of land degradation indicators using metrics derived from remote sensing technology. These outputs can be employed to inform land management and investment decisions, improve reporting to the United Nations Convention to Combat Desertification (UNCCD) and the Global Environment Facility (GEF), and support monitoring the achievement of Sustainable Development Goal (SDG) target 15.3, Land Degradation Neutrality (LDN). A series of reports, of which this is the first, will be produced in line with these objectives. In this report, we compare a number of datasets and vegetation indices at multiple spatial scales to assess their ability to depict photosynthetic capacity and ultimately to monitor changes in primary productivity, which could function as indicators of land degradation or improvement.

On-the-ground partners collect data in Tanzania.
© Benjamin Drummond

In this report, we evaluate remotely sensed techniques for assessing changes in productivity. We evaluate trends in primary productivity, as well as trends in primary productivity independent of climate variability, a necessity of LDN determination in areas where water availability limits plant growth. The methods assessed for doing this involve developing relationships between Normalized Difference Vegetation Index (NDVI) and environmental drivers (precipitation and soil moisture) at different temporal scales (8-days, bi-monthly, and monthly by year). Then, by analyzing the regression residuals we determine trends in primary productivity independent of climate. We use negative trends in these regression residuals as an indicator of decline in productivity independent of precipitation or soil moisture variability. Conversely, positive trends determined by our residual analysis would indicate areas of land improvement in terms of productivity.

The long term coarse to medium spatial resolution analysis presented in this report is key for identifying trends in primary productivity, but this analysis is limited in its ability to identify land degradation, especially in mountainous regions, or highly fragmented landscapes with particular geomorphological features where a finer spatial resolution is needed. To address that important component of land degradation, we are forming 50 cm satellite images, for four pilot countries (Senegal, Tanzania, Uganda, and Tanzania) of all areas where negative or positive residual trends have been determined. In conjunction with data from sources like social surveys and plot monitoring, these datasets will allow users to better understand the drivers of these residual trends. We will report on these findings in our second report.

ACKNOWLEDGEMENTS

We are grateful to the members of the Science Advisory Board for their advice and input on this report:

STEFANIE HERRMANN	University of Arizona
GRACIELA METTERNICHT	University of New South Wales
SARA MINELLI	UNCCD Secretariat
MARC PAGANINI	ESA Centre for Earth Observation

We also thank the Project Steering Committee for their guidance:

SANDY ANDELMAN	Organization for Tropical Studies
MICHAEL CHERLET	Joint Research Centre, European Commission
ANNETTE COWIE	Scientific and Technical Advisory Panel to the Global Environment Facility
STEPHEN MUWAYA	Ministry of Agriculture, Animal Industry, and Fisheries, Uganda
LENNART OLSSON	Lund University
ALEX ZVOLEFF	Conservation International

Substantial inputs to review and revision, and contributions to the appendices, were made by:

MARIANO GONZALEZ ROGLICH	Conservation International
ALEX ZVOLEFF	Conservation International

We are also grateful for the inputs throughout the revision process that were made by:

JOHN LEE DAVID	NASA
KATHERINE MELOCIK	NASA
MONICA NOON	Conservation International
TRISTAN SCHNADER	Conservation International

TABLE OF CONTENTS

I. CONTENTS

II. LIST OF FIGURES

II. LIST OF FIGURES

III. LIST OF TABLES

III. LIST OF TABLES

Aerial view of agricultural fields on a mountain, Rwanda. © Rod Mast

IV. LIST OF APPENDIX FIGURES

IV. LIST OF APPENDIX FIGURES

A commerical pineapple operation just outside of Okwabena in southern Ghana. © Benjamin Drummond

V. TABLE OF ACRONYMS

V. TABLE OF ACRONYMS

AVHRR	Advanced Very High Resolution Radiometer
BRDF	Bidirectional reflectance distribution function
CBD	Convention on Biological Diversity
CI	Conservation International
ERA-I	European Reanalysis Interim
ESA	European Space Agency
EUE	Energy-use efficiency
EVI	Enhanced vegetation index
FAO	Food and Agriculture Organization of the United Nations
GEF	Global Environment Facility
GIMMS3g	Global Inventory Modeling and Mapping Studies, 3rd generation (NDVI dataset)
GLADA	Global Assessment of Land Degradation and Improvement
GLASOD	Global Assessment of Soil Degradation
GMAO	NASA's Global Modeling and Assimilation Office
GOME-2	Global Ozone Monitoring Experiment–2
GPCP	Global precipitation climatology project
GPP	Gross primary productivity
GSFC	Goddard Space Flight Center
HadISDH	Met Office Hadley Centre led project utilizing ISD Humidity data
JRC	Joint Research Centre of the European Union
LADA	Land Degradation in Drylands
LDN	Land Degradation Neutrality
MERRA-2	Modern-Era Retrospective analysis for Research and Applications, Version 2
MERIS	Medium Resolution Imaging Spectrometer
MODIS	Moderate Resolution Imaging Spectroradiometer
MODIS CMG	MODIS Climate Modeling Grid
NASA	National Aeronautics and Space Administrations
NCEP	National Centers for Environmental Prediction
NDVI	Normalized difference vegetation index
NDVI-3g	Normalized difference vegetation index 3rd generation
NIR	Near-infrared
NOAA	National Oceanic and Atmospheric Administration
RESTREND	Residual Trend Analysis
RUE	Rain use efficiency
SDG	Sustainable Development Goals
SeaWIFS	Sea-Viewing Wide Field-of-View Sensor
SIF	Solar-Induced chlorophyll Fluorescence
SLM	Sustainable Land Management
SPOT-4	Satellite Pour l'Observation de la Terre, Version 4
UNFCCC	United Nations Framework Convention on Climate Change
SPOT-5	Satellite Pour l'Observation de la Terre, Version 5
UNCCD	United Nations Convention to Combat Desertification
UNEP	United Nations Environment Program
USGS	United States Geological Survey
UTM	Universal Transverse Mercator coordinate system
VI	Vegetation Index
VIIRS	Visible Infrared Imaging Radiometer Suite
VS	Vital Signs

VI. INTRODUCTION

VI. INTRODUCTION

Land degradation has been highlighted as a key development challenge by numerous international bodies, including the United Nations Convention to Combat Desertification (UNCCD), the Convention on Biological Diversity (CBD), the United Nations Framework Convention on Climate Change (UNFCCC), and the Sustainable Development Goals (SDGs). The UNCCD aims to avoid, reduce, and reverse land degradation, especially desertification and deforestation, by providing support to sustainable land management (SLM). SLM implements practices that maintain vegetative cover, build soil organic matter, make efficient use of inputs, such as water, nutrients and pesticides, and minimize off-site impacts (Bierbaum et al. 2014). The Global Environment Facility (GEF) was designated as a financial mechanism for the UNCCD in 2003, with activities initially focused on the SLM operational program, and, in 2006, its Land Degradation focal area was established. The UNCCD distinguishes what to measure (indicators) from how it is assessed (metrics). In the context of Land Degradation Neutrality (LDN), target 15.3, the UNCCD has identified 3 indicators: land cover, carbon stocks above and below ground, and land productivity or functioning of the land.

UNCCD TARGET 15.3 INDICATORS:

- **LAND COVER**
- **CARBON STOCKS**
- **LAND PRODUCTIVITY**

The UNCCD thus uses land cover and land productivity as two of the three indicators to monitor land degradation. Land cover includes distinct types of land cover, as typically represented in a land cover class map. Land productivity dynamics are based on long-term fluctuations and current efficiency levels of phenology and productivity factors affecting standing biomass conditions (UNCCD 2013). Target 15.3 of the Sustainable Development Goals (SDGs) also use land cover and land cover change, together with land productivity as sub-indicators to track progress towards LDN (UN 2016).

For the GEF, achievement of the overall goal of the Land Degradation focal area is measured through "change in land productivity" using, as a proxy, gross primary productivity (GPP), which is estimated through the remotely sensed Normalized Difference Vegetation Index (NDVI), a proxy for photosynthetic capacity. In this report, we evaluate using NDVI data coupled with solar-induced chlorophyll fluorescence, to provide GPP information at spatial scales from 8 km to 250 m to identify areas of degraded lands in Senegal, Uganda, Kenya, and Tanzania. We also evaluate different NDVI trend analysis techniques in their ability to capture temporal variations in primary productivity which could help identify areas of land degradation and improvement.

The GEF uses land degradation preliminary assessments to prioritize investments. The GEF benefits index (GBI) for the Land Degradation Focal Area is based on three indicators: area affected by LD, total dryland area, and vulnerable population (GEF 2015). Further, to measure the impact of interventions, GEF-funded SLM projects report on the same set of metrics. If land cover does not change, but the area in question is being degraded, this can be identified for some types of degradation by analysis of NDVI through its coupling to gross primary production. If the land cover of an area does change, this resulting change can also be expressed in terms of change in gross primary productivity, enabling quantitative analyses of the land cover change.

Remotely sensed data products derived from satellite measurements come in several bands of the electromagnetic spectrum. NDVI and other spectral indices use bands in the visible and near-infrared wavelengths to derive a product that is in principle indicative of variations in levels of greenness. When using satellite-derived products, it is important to consider sensor and image characteristics such as: image size, region of the earth from which images are acquired, spatial resolution, number of bands and wavelengths detected, spectral characteristics of the bands, frequency of image acquisition, and the date of origin of the sensor (Strand et al. 2007).

The reviews conducted by Yengoh et al. (2014) and Higginbottom and Symeonakis (2014) recommend using NDVI as an indicator of changes in land productivity and as a proxy for monitoring land degradation.

NDVI has been used extensively in research on primary production, land use and land cover change, drought, desertification, soil erosion, vegetation burned areas, biodiversity monitoring and conservation, and soil organic carbon (Higginbottom and Symeonakis 2014, Yengoh et al. 2014). Recent improvements and the longer time series of fundamental NDVI datasets call for development and testing of new and improved methods and tools for using NDVI or other spectral indices as a means to understanding the status of degradation and as metrics for reporting. Such a harmonization approach is closely aligned with the effective implementation of LDN and may assist UNCCD and GEF in identifying effective actions in SLM projects.

However, some fundamental barriers must be overcome before the use of NDVI or other spectral indices as proxies of monitoring achievement of LDN. The recognition that a minimum set of standard monitoring methods will lead, under certain circumstances, to "false positives", call for additional in-situ national and sub-national, both quantitative and qualitative data and information, to aid interpretation while also accommodating variability in the causes and consequences in land degradation among countries.

There is a large body of evidence in the literature on the usefulness of NDVI data for detecting and monitoring areas of potential land degradation, which should be then validated with field and local data to obtain robust estimates of trends at the local level. For example, the UNCCD monitoring and reporting approach recommends that global indicators are supplemented by national (or sub-national) level indicators to strengthen the interpretation of the global indicators. While this is encouraging regarding the potential for regular use of NDVI-based data for national reporting on land degradation trends to the GEF and UNCCD, this evidence comes from studies that have used a wide range of data sources. Yengoh et al. (2014), commissioned by the Scientific and Technical Advisory Panel (STAP) of GEF, thoroughly reviews this body of work, as does a recent paper by Higginbottom and Symeonakis (2014). These papers conclude that this body of evidence is significant; however, it has not yielded simple guidance on data, methods or tools for countries to use to set baselines and for reporting to the UNCCD or the GEF, or for the latter to use in priority setting. This is related to several critical factors: lack of standardized and harmonized datasets, lack of methods for using datasets, lack of tools and specific guidance of limitations of the datasets and on how to use both the datasets and tools, and limited capacity of governments and stakeholders in collecting, analyzing, interpreting and reporting.

VI.1. PREVIOUS LAND DEGRADATION ASSESSMENT EFFORTS

Early assessments of land degradation, such as the Global Assessment of Soil Degradation (GLASOD), were based on compilations at small scale of expert opinion (Oldeman et al. 1990). The results of the GLASOD study, being based on expert judgment, are unrepeatable, subjective and unreliable as more systematic quantitative information is needed to support assessment, policy and action on land degradation (Bai et al. 2008a). To meet this need at global scale under the FAO (Food and Agriculture Organization of the United Nations) / UNEP (United Nations Environment Program) program, Land Degradation in Drylands (LADA), Bai et al. (2008b) undertook a Global Assessment of Land Degradation and Improvement (GLADA) by analyzing linear trends of climate-adjusted NDVI 8km data from Global Inventory Modeling and Mapping Studies (GIMMS). Since the early 1980s, links have been established between land degradation and a decline in primary productivity or change in land cover (Wessels et al. 2004, Hein and de Ridder 2006, Prince et al. 2007, Wessels et al. 2007, Bai et al. 2008a). The difficulty is to discount false alarms raised by other factors, notably fluctuations in rainfall or rising temperatures.

GLADA, the first quantitative assessment of global land degradation, aimed to identify and delineate "hot spots of land degradation, and their counterpoint - bright spots of land improvement." The study reduced the number of false alarms by screening the NDVI data with rain use efficiency (RUE) and energy-use efficiency (EUE). RUE is defined as the ratio between integrated NDVI (as proxy of primary productivity) and annual precipitation and EUE is derived as the ratio of NDVI and annual accumulated temperature. The picture revealed by GLADA suggested that about 24% of the global land area was affected by land degradation between 1981 and 2003. Humid areas accounted for 78% of the global degraded land area, while arid and semiarid areas accounted for only 13%. Cropland and rangelands accounted for 18% and 43%, respectively, of the 16% of global land area where the NDVI increased.

Bai et al. (2008a) observed that, in different locations, decreases in NDVI were both positively and negatively correlated with changes in population density, as well as with both increases and decreases in poverty. They emphasized that NDVI can only be used as a proxy for land degradation and that it reveals nothing about the type of degradation or its drivers. However, as noted by Fensholt and Rasmussen (2011) as well as Hein et al. (2011), the results based on RUE are not consistent since the proportional assumption between NDVI and precipitation does not hold. Since GLADA was conducted, new and improved datasets and studies have emerged, together with opportunities to combine low-resolution, medium-resolution and high-resolution satellite datasets to better understand land degradation (Fensholt et al 2013, Ibrahim et al. 2015). These recent studies infer status of an ecosystem by correcting for climate components in the NDVI trends using residual trend analysis (RESTREND) (Evans and Geerken 2004).

VI.2. SATELLITE DATA SOURCES FOR MONITORING LAND DEGRADATION

National Oceanic and Atmospheric Administration (NOAA) Advanced Very High Resolution Radiometer (AVHRR) data have the longest temporal record, extending from July 1981 to the present. These data include three thermal bands as well as reflectance bands in the red and near-infrared (NIR). The latter allow calculation of NDVI and other two-band spectral indices; the former allow estimation of and corrections for cloud contamination and atmospheric effects. AVHRR data have a 4 km resolution and are mapped to 8 km grid cells. While originally intended for atmospheric and oceanic study, AVHRR data have formed the basis for global-change and bio-climatology research from the 1980s to the present. They revealed spatially-continuous, seasonal, and inter-annual patterns of vegetation dynamics and land temperature for the first time; quantified land gross primary productivity; and identified how phenomena, such as the El Niño Southern Oscillation affect climate.

Currently, the NDVI3g data archive is the only global coverage dataset spanning 1981 to the present day that is subject to continuous validation (Pinzon and Tucker 2014). Thus, AVHRR NDVI data provide a longer time series; however, their overall usefulness to assess land degradation is limited because of their coarse (8 km) resolution, in comparison with 250 m NDVI data from the MODIS instruments. AVHRR NDVI data are useful at the global to regional scale for a 36-year period, from 1982 to 2017. AVHRR data are expected to continue beyond 2020, with AVHRR instruments flying now on MetOps-2 and after 2018 on the MetOps-3 polar-orbiting meteorological satellites.

The MODIS program started in 1999, and NASA is committed to continued operation and delivery of MODIS data from the Aqua and Terra satellites through 2017. Since early 2014, there has been overlapping data from Suomi-NPP VIIRS. VIIRS has similar characteristics to MODIS useful for generation of photosynthetic potential and this

program is planned to run beyond 2030. NASA plans continuation of compatible data with MODIS by undertaking the processing and distribution of VIIRS NDVI data.

This activity will continue to provide daily or near-daily surface reflectance as well as 8-day and 16-day NDVI and Enhanced Vegetation Index 2 (EVI-2) data globally at a 300-m resolution. The NASA GIMMS program is committed to continuing its research to harmonize surface reflectance and photosynthetic capacity data provided by these sources through 2017 and beyond.

The VEGETATION-1 and -2 sensors on board SPOT-4 and SPOT-5 satellites provided data from 1998 to 2014. VEGETATION provides reflectance data for the red, NIR and middle-infrared at a resolution of 1.2 km. The SPOT program has produced several time series data sets, including surface reflectance and global NDVI. VEGETATION data do not include any thermal bands, and thus have less potential for correcting for atmospheric effects and clouds. The PROBA-V sensor, launched in early 2014, provides continuity to the VEGETATION 1 and 2 sensors measuring in the same bands, although with improved spatial resolution of 300 m in the visible and near infrared, and 600 m in the middle-infrared bands. PROBA-V is planned to fill a short-term gap before Sentinel 3 is launched later this decade. Between 2002 and 2012, MERIS, on board ENVISAT provided images at 300m resolution data set. The ESA plans to continue PROBA-V through 2018 and then provide relevant data mainly via Sentinel-3 series, committed through 2035 and beyond as part of the European Copernicus Program.

By mid 2017, we will have another GPP option with a 30 m NDVI time series from Landsat-8 and Sentinel-2a & -2b data. Landsat historical data is not enough to undertake historical phenological analyses at a global scale. However, a Landsat-8 and Sentinel-2 a, and Sentinel 2b "harmonized" product is now providing a 30 m global visible, near-infrared, and short-wave infrared data set with a 3.7 day repeat frequency at the equator (Mandanici and Bitelli 2016). With the launch of Landsat-9 in 2020, the repeat frequency will fall to 3.0 days. This activity is an ESA-NASA-USGS collaboration.

In summary, there are currently three data options for a global assessment of historic trends in GPP that can be used for land degradation studies: (1) AVHRR data that started in 1981; (2) the SPOT VEGETATION, PROBA-V and Sentinel-3 series, which started in 1998; and (3) MODIS and VIIRS data series which started in 2000. By using multiple spatial resolutions, we are able to (1) confirm observations and measurements made using the coarse resolution time series; and (2) better understand how different types of changes on the ground are manifested in moderate-coarse resolution data. Moving forward, the MODIS-VIIRS continuum and the "harmonized" Landsat-Sentinel-2 data are the better satellite time series data because of their inter-calibration, atmospheric processing, and spatial resolutions.

VI.3. OBJECTIVE

The objective of this project is to provide guidance, methods, and a toolbox to support assessing and monitoring status toolbox to support assessing and monitoring the status of land degradation indicators using metrics derived from remote sensing technology. These outputs can be employed to inform land management and investment decisions as well as improve reporting to the UNCCD and the GEF, and support monitoring the achievement of LDN, SDG target 15.3. A series of reports, of which this is the first, will be produced in line with these objectives. In this report, we compare a number of datasets and vegetation indices at multiple spatial scales in order to assess their ability to depict photosynthetic capacity and ultimately to monitor changes in primary productivity, which could function as indicators of land degradation or improvement.

VII. COMPARING VEGETATION INDICES

VII. COMPARING VEGETATION INDICES

VII.1. INTRODUCTION

Vegetation indices derived from satellite data are one of the principal sources of information for monitoring and assessment of the Earth's vegetative land cover and primary productivity, since they are surrogates for photosynthetic capacity or potential (Sellers 1985 and 1987; Myneni et al. 1995). To evaluate the suitability of spectral vegetation indices to quantify changes in GPP, we analyzed data from a range of sensors, at a range of spatial and temporal resolutions. We propose to assess changes in primary productivity, to point to areas of potential land degradation, using vegetation indices derived from satellite data sets that meet the following criteria:

VEGETATION INDICES MUST BE DERIVED FROM SATELLITE DATA SETS THAT MEET THE FOLLOWING CRITERIA:

- **THEY ARE FREELY AVAILABLE;**
- **THEY ARE WELL DESCRIBED IN THE SCIENTIFIC LITERATURE;**
- **THEY ARE CURRENT INTO 2017 AND WILL BE CONTINUED BEYOND THIS TIME;**
- **THEY ARE PRODUCED IN A CONSISTENT & CALIBRATED NON-STATIONARY FASHION;**
- **THEY HAVE GLOBAL COVERAGE;**
- **THEY HAVE A FREQUENCY OF OBSERVATION THAT IS SUFFICIENTLY DENSE TO CHARACTERIZE SEASONAL AND INTER-ANNUAL DYNAMICS; AND**
- **THEY HAVE SPATIAL AND SPECTRAL PROPERTIES THAT ENABLE THE ESTIMATION OF LAND DEGRADATION AT NATIONAL AND SUB-NATIONAL LEVELS.**

We focus in this report on the indicator of land productivity, and more specifically, on gross primary production by measurement or modeling, including solar-induced chlorophyll fluorescence.

We emphasize measurement over modeling because it provides more spatial detail. Although two current GPP modeling efforts use satellite data in part, the other methods do not. There is no consensus among the various estimates of global GPP and a wide range of estimates exist. There is disagreement on the amplitude, inter-annual variability, and trend of global GPP. There is an urgent need to improve estimates of GPP to quantify carbon uptake on land (Anav et al. 2015) and to map change in productivity as one component of land degradation.

- Two observation-based GPP approaches have been investigated: Eddy-covariance flux tower observations from ~180 specific locations are extrapolated globally based upon satellite measured absorbed photosynthetically-active radiation (NDVI is very highly correlated to APAR) and global climate fields. GPP is then predicted by a set of multiple linear regressions (Beer et al. 2010, Jung et al. 2011). The spatial resolution of this approach is 0.5° x 0.5° or roughly 50 x 50 km at monthly time steps; and

- Data-driven satellite observations using time series MODIS satellite observations and other climate variables. A light-use efficiency model is coupled to daily photosynthetically-active radiation and other climate variables to produce GPP estimates at a scale of 1 km at 8-day, monthly, and annual time steps (Zhao and Running 2010). Uncertainties in the MODIS GPP product result from uncertainties in fAPAR, leaf area index, daily meteorological data, the GPP algorithm, and its parameters (Zhao et al. 2005).

An advantage of these two approaches is that the satellite observations provide realistic surface conditions of vegetation photosynthetic capacity, vegetation disturbances, vegetation recovery, and human management. As noted by Anav et al. (2015), if both remotely sensed GPP and modeled GPP are perfect and their respective input data accurate, modeled GPP will tend higher, because the modeling approach neglects disturbance that will lower GPP.

On the observation-driven GPP approach, sustained land imaging is now providing global 30 m multi-spectral imagery from "harmonized" Landsat-8, Sentinel-2a, and Sentinel-2b data with a repeat frequency of 3.7 days at the equator and more frequently towards the poles (Mandanici and Bitelli 2016). This will lead to improving the observation-based estimates of GPP by enabling a 30-60 m refinement of the MODIS-based GPP method, including the opportunity for 1:1 comparisons of predicted GPP with actual ground measurements of the same. MODIS-like imagery will also be continued beyond 2035 by the VIIRS instruments on the Joint Polar Satellite System's satellites of NASA and NOAA, so VIIRS 375 m time series data will continue the MODIS GPP 1 km product.

In addition to the observation-driven approaches, there are also process-based land carbon models. Sitch et al. (2015) summarize the process-based land carbon GPP models that took part in the TRENDY project. Anav et al. (2015) review three of the TRENDY models that used common input variables: observed CO_2 concentrations, the same land cover change, and the same 6-hourly climate data from the Climate Research Unit and National Center for Environmental Prediction climate forcings (Wei et al. 2014). Anav et al. (2015) also review four Earth System Models from the Fifth Climate Model Inter-comparison Project (CMIP5) that used common simulation and output protocols. These three models were forced by the same greenhouse gas and sulfate aerosol data, by the same total solar irradiance data, by the same volcanic aerosol forcing data, and by the same land use and land cover changes (Taylor et al. 2012). These six models resulted in Table 1 in Anav et al. (2015) (Table 1).

	Offline (TRENDY)			Online (CMIP5)			
	CLM4CN	JULES	ORCHIDEE	CESM1-BGC	HadGEM2-ES	IPSL-CM5A-MR	NorESM1-ME
Spatial resolution (longitude×latitude)	0.5°×0.5°	1.85°×1.25°	0.5°×0.5°	0.9°×1.25°	1.875°×1.25°	2.5°×1.25°	2.5°×1.9°
Land area (60°S–90°N)	1.359E+14 m^2	1.333E+14 m^2	1.343E+14 m^2	1.347E+14 m^2	1.335E+14 m^2	1.381E+14 m^2	1.347E+14 m^2
Number of PFTs	16	5	13	15	5	13	15
Dynamic vegetation	N	N	N	N	Y	N	N
N Cycle	Y	N	N	Y	N	N	Y
Land component	Valid only for the online models			CLM4CN	JULES	ORCHIDEE	CLM4CN
Atmospheric forcing	CRU-NCEP			CAM4	HadGEM2	LMDZ	CAM4-Oslo
Reference	Oleson et al. [2010]	Clark et al. [2011]	Krinner et al. [2005]	Gent et al. [2011]	Collins et al. [2011]	Dufresne et al. [2013]	Bentsen et al. [2013]

Table 1. From Anav et al. (2015, Table 1): "Summary of the Land Models Used with the Associated Original Resolution and Main Features Controlling the Terrestrial Carbon Cycle".

An important point shown in Table 1 is the spatial resolution of the various Earth System models that do not use satellite data range from 50 x 50 km (0.5°×0.5°) to 250 x 200 km (2.5°×2°). The modeling GPP estimations have no applicability for land degradation research because of their coarse resolution and they have no mechanism for capturing land surface disturbance. Only observation-based GPP offers the possibility of using GPP estimates for land degradation mapping for these two reasons.

In addition to the approaches for observation-based and process-based modeling described above, a direct observation method of quantifying GPP has been proposed using solar-induced chlorophyll fluorescence (Joiner et al. 2011, Frankenburg et al. 2011, Guanter et al. 2014, Zhang et al. 2016, Wood et al. 2017, Goulas et al. 2017). The advantage that solar-induced fluorescence has over other approaches is it is a flux tied to photosynthesis (i.e., g C m^{-2} day^{-1}; Maxwell and Johnson 2000). Thus, when SIF is measured, photosynthesis is occurring. The disadvantage of SIF is that it must be measured in the electromagnetic spectrum where no down-welling solar spectral irradiance is present. This can only be accomplished within Fraunhoffer lines that have a narrow bandwidth (< one Angstrom) or within the Oxygen-A and Oxygen-B bands which area also narrow and have other confounding problems (Joiner et al. 2011. The very narrow Fraunhoffer line bandwidth means SIF observations will never be less than a few hundred meters spatial resolution. For example, GOSAT SIF data are 100 x 100 km (Yokota et al. 2009) and GOME-2 SIF data are 40 x 80 km (Joiner et al. 2011). The European Space Agency's FLEX mission, scheduled for launch in 2022, will be a mission dedicated to investigating SIF form orbit and will have a spatial resolution from 0.3 to 1.0 km resolution (Vincent et al. 2016). With our approach of using NDVI & SIF together, we are able to apply our results at 250 m. With the "harmonization" of Landsat-8, Sentinel-2a, and Sentinel-2b to a 30 m multi-spectral time series data set, we will be able to apply our NDVI-SIF GPP method to 30 to 60 m with the Landsat-8 and Sentinel-2 combined data (Mandanici and Bitelli 2016).

VII.2. ANALYTICAL METHODS

In this chapter, we evaluate the potential of vegetation indices to estimate gross primary production as captured by solar-induced chlorophyll florescence. We discuss here only those vegetation indices for which current and freely available global data exist. These datasets are the NDVI, and the two MODIS versions of the Enhanced Vegetation Index (EVI): a two-channel (EVI-2) and three-channel (EVI-3) product.

Using data from NASA's MODIS instruments in combination with GOME-2 chlorophyll fluorescence data, referred to as solar-induced fluorescence or SIF data, we determine how well vegetation indices are able to capture photosynthesis. We use growing-season integrals from GOME-2 SIF data as a measure of gross primary productivity, and then correlate these findings with the growing-season integral of NDVI. Comparisons are made for the 2007 to 2015 overlap period for SIF and the vegetation indices data from MODIS, the 2007-2015 overlap period for SIF and the NDVI3g data set, and for the 2007-2010 overlap period between SIF and vegetation indices derived from SeaWiFS data. Collection of SeaWiFS data stopped in 2011 when the satellite malfunctioned. All the data have been aggregated to the coarsest resolution (~50km) so that the effects of different spatial resolution are excluded in the comparison.

Per pixel quality and cloud condition information in all VI data products allow for correction of most cloud contaminated VI signals. A temporal gap-fill algorithm is applied to all VI (NDVI, EVI-2, EVI-3) time series data. A climatological average is computed for each pixel using only good quality VI observations within each year. We use the correspondent seasonal average to fill the gaps caused by flagged values at each pixel. Fortunately, this happens less than one percent (<1%) of the time (Pinzon & Tucker 2014, Fensholt and Proud 2012). The SIF data has been gridded to 2° spatial-resolution and 15 day temporal-resolution. Quality assurance was conducted to filter out cloudy data and failed retrievals as described in Joiner et al (2014).

As detailed in Joiner et al. (2014), the SIF signal can still be detected through moderately cloudy conditions. Placing stricter limits reduces coverage and increases noise in gridded SIF averages.

VII.2.A. THE VEGETATION INDICES

The normalized difference vegetation index (NDVI), (Equation 1) is the ratio of the difference between the near-infrared band (NIR) and the red band (R) and the sum of these two bands (Rouse et al. 1974, Deering 1978) and reviewed in Tucker (1979). The MODIS Land Discipline group has developed two versions of the Enhanced vegetation index (EVI), a two-channel (EVI-2) and three-channel (EVI-3) product for MODIS data from 2000 to 2016. EVI-2 (Jiang et al. 2008) & EVI-3 (Huete et al. 2002) are defined in equations 2 and 3 respectively.

$$NDVI = \frac{NIR - RED}{NIR + RED} \quad (1)$$

$$EVI2 = 2.5 * \frac{NIR - RED}{1 + NIR + 2.4 * RED}$$

$$= NDVI * 2.5 * \frac{NIR + RED}{1 + NIR + 2.4 * RED} \quad (2)$$

$$EVI3 = 2.5 * \frac{NIR - RED}{1 + NIR + 6 * RED - 7.5 * BLUE}$$

$$= NDVI * 2.5 * \frac{NIR+RED}{1+NIR+6*RED-7.5*BLUE} \quad (3)$$

Where 'RED' is the red channel, 'NIR' the near infrared channel, and 'BLUE' the blue channel. The 3-channel enhanced vegetation index (EVI-3) is reported to be "optimized to enhance the vegetation signal with improved sensitivity in high biomass regions and improved vegetation monitoring through a de-coupling of the canopy background signal and a reduction in atmosphere influences" through its heritage from the soil-adjusted vegetation index (SAVI) and the atmospherically resistant vegetation index (ARVI) (Huete et al. 2002). However, Vargas et al (2013) evaluating VIIRS vegetation indexes reported that EVI-3 exhibits artifacts (large positive values) that are not related to spatial features of the landscape where one would expect low or negative EVI values and they suggested that the cause of the problem is that certain combination of spectral bands with the negative coefficient of the blue channel in the denominator (see equation 3), are out of domain of EVI-3. This issue is resolved using EVI-2 (Jiang et al. (2008) in all these cases and also by compositing the data. We evaluated the relative performance of NDVI, EVI-2, and EVI-3 in relation to photosynthesis as measured by the GOME-2 SIF data.

VII.2.B. NDVI, EVI2, EVI3 AND RED ABSORPTION COMPARISON

Data Source	Spatial Resolution(s)	Temporal Resolution(s)	Use
MODIS CMG	5 km	16-day composite	Calculation of NDVI, EVI2, EVI3 from RED, NIR, BLUE channels from MODIS climate modeling 5 km grid data for 2000 to 2015.
SeaWiFS	4 km	Bi-monthly composite	Calculation of NDVI, EVI2, EVI3 from RED, NIR, BLUE channels from SeaWIFS 4 km grid data for 1998 to 2010.

Table 2. Sources of satellite vegetation indices data and their characteristics used in the comparison of NDVI, EVI2, EVI3 and Red reflectance.

We evaluated the performance of only operational vegetation indices: NDVI, EVI-2, and EVI-3. We used sensors which had the spectral bands required for their computation. These sensors were MODIS and SeaWiFS (Table 2). For the first comparison, we computed the three vegetation indices from the SeaWiFS data and compared them to the spectral response of the red absorption band for the entire vegetated surface of the planet. We used the red band for this comparison, because chlorophyll strongly absorbs the red portion of the electromagnetic spectrum during photosynthesis, and consequently the down-welling red solar flux from the sun is a major driver of GPP.

VII.2.C. VEGETATION INDICES AND CHLOROPHYLL FLUORESCENCE RELATIONSHIPS

We analyzed SeaWiFS data for 2007 to 2010, the overlapping period between the SeaWiFS and MODIS sensors, and compared the SeaWiFS vegetation indices with coincident GOME-2 SIF data for 22 selected areas with all areas having dimensions of ~40,000 km^2 (Figure 1). The best available estimates of GPP are from direct measurement of carbon dioxide exchange by so called flux towers (Baldochi et al. 2012). However, these generally sample small areas. We selected 15 sites in North America with a range of GPP values from very high to moderate. We also used seven locations we had analyzed previously in Russia (Yoshida et al. 2015). This brought the total number of sites to 22. We used the SIF data to represent gross primary production (Joiner et al. 2014).

We determined dates of start and end of the growing season by computing mean weekly two-meter height MERRA-2 temperature (Reichle et al. 2016) and NDVI values by sensor at the pixel level for the start of the growing season and the end of the growing season by year.

The growing seasons were determined by the period for which temperature was >273K and NDVI > 0.1. Low temperatures (near or below freezing) are generally sufficient to reduce GPP to near or equal to zero. However, in areas where temperatures are above freezing of the main part of growing season, it is more challenging to estimate the initiation (spring) and the decline of photosynthesis (autumn). As a result, GPP is overestimated at low productivity sites (Turner et al. 2006). We try to reduce these abnormal values with a fixed NDVI threshold as suggested by Fensholt et al (2013), although an optimal seasonal parameterization could vary as a function of vegetation land cover. The period determined by this analysis was used as the growing season period for each particular location throughout the rest of the study. Using this period as the growing season, we calculated growing season integrals of vegetation indices NDVI, EVI-2, and EVI-3 and regressed them against growing season integrals of SIF data (Table 3) to evaluate indirectly the indices' relationships to GPP. An advantage of this approach is that SIF, being a flux tied to photosynthesis, is sensitive to dynamic ranges in physiological functioning and light-use efficiencies (LUEs), obtaining better constraints on spatiotemporal variations in GPP (Anav et al. 2015).

Data Source	Spatial Resolution(s)	Temporal Resolution(s)	Use
MODIS MOD09Q1	250 km	8-day composite	• Calculation of NDVI, EVI2, EVI3 from RED, NIR, BLUE channels from MODIS climate modeling 5 km grid data for 2000 to 2015. • Derive 2° by 2° spatial average correspondent VIs products for 2007 to 2015.
MODIS CMG	5 km	16-day composite	• Calculation of NDVI, EVI2, EVI3 from RED, NIR, BLUE channels from MODIS climate modeling 5 km grid data for 2000 to 2015. • Derive 2° by 2° spatial average correspondent VIs products for 2007 to 2015.
SeaWiFS	4 km	Bi-monthly composite	• Calculation of NDVI, EVI2, EVI3 from RED, NIR, BLUE channels from SeaWIFS 4 km grid data for 1998 to 2010. • Derive 2° by 2° spatial average correspondent VIs products for 2007 to 2010. Comparisons to SeaWiFS were made for 2007 to 2010, since SeaWiFS ceased functioning in early 2011.
GOME-2	40 x 80 km	8-day and Bi-monthly composite	• Fluorescence grid data version 26 (V26) representing gross primary production after (Joiner et al. 2014). Retrievals of fluorescence are from the GOME-2 instrument on MetOp-A and MetOp–B from 2007 to 2016 and beyond.

Table 3. Sources used in analysis of vegetation indices and chlorophyll fluorescence relationships.

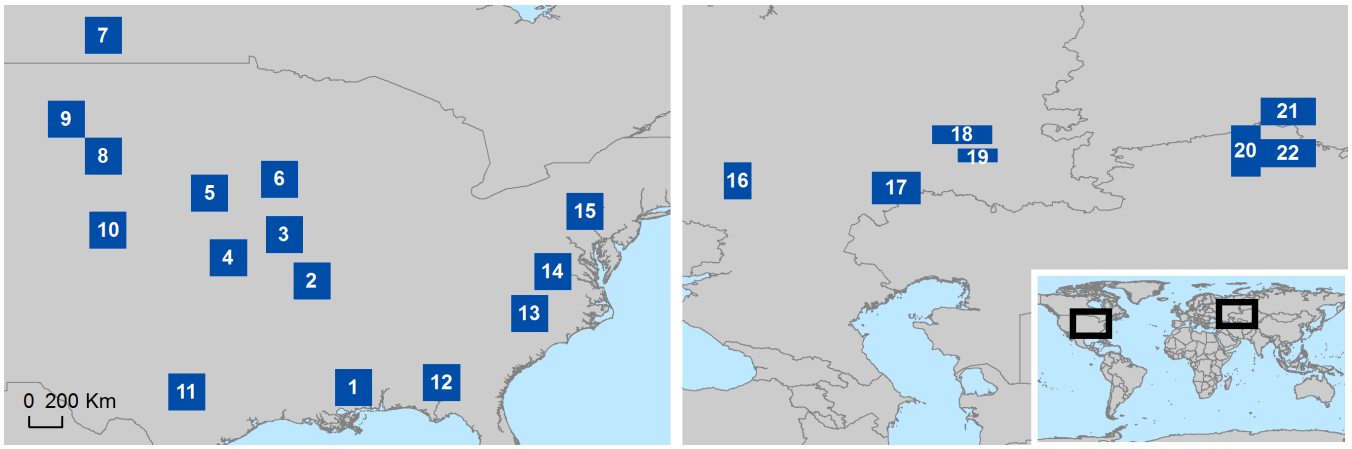

Figure 1. The 22 areas from which NDVI and SIF data were compared for their common period of 2007 to 2015.

VII.3. RESULTS

VII.3.A. NDVI, EVI2, EVI3 AND RED ABSORPTION COMPARISON

Chlorophyll strongly absorbs the red portion of the electromagnetic spectrum during photosynthesis, and consequently the down-welling red solar flux from the sun is a major driver of gross primary productivity. To convey this idea, we compute the joint probability density function (pdf) between each vegetation index and red absorption using one million points randomly selected from the entire (global 13 year) SeaWiFS data set. When plotting the three different joint pdfs, their different behaviors can be easily identified (Figure 2). NDVI is less asymptotic than the EVI-2 and much less asymptotic than the EVI-3 with respect to the percent of red light absorbed by green vegetation. The more linear behavior between NDVI and red absorption could be interpreted as an indicator of the superiority of NDVI to describe photosynthetic capacity, as the NDVI does not saturate at higher levels of red absorption.

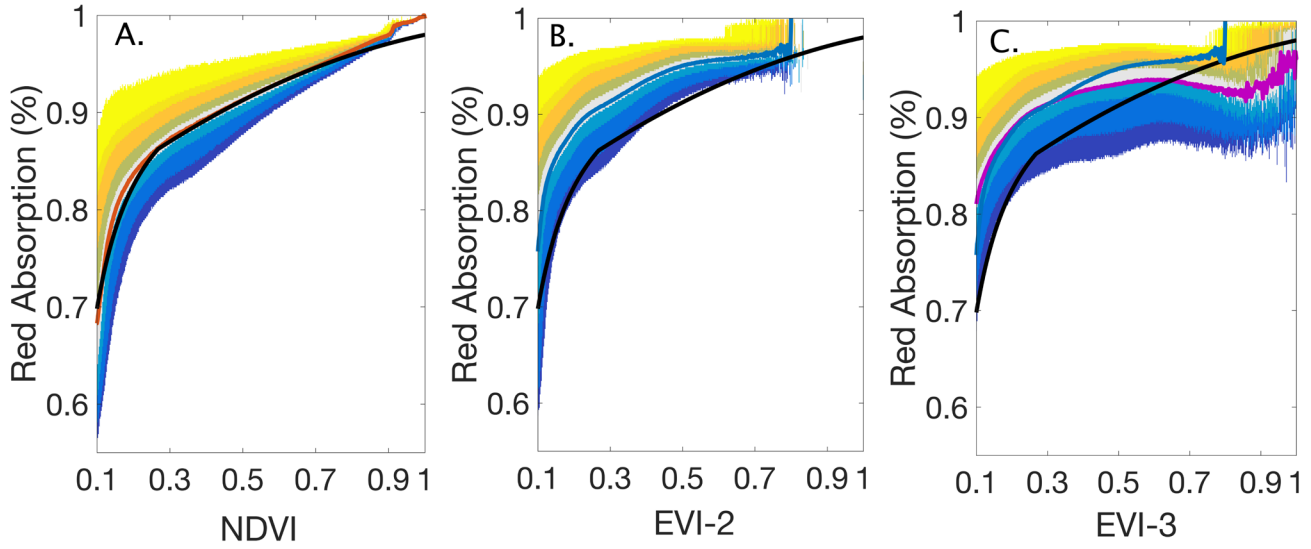

Figure 2. Comparison of the distribution of SeaWiFS NDVI, EVI-3, and EVI-2 to red absorption by vegetation at 5, 10, 25 (blue), 40-60 (gray), median values (NDVI - red line, EVI-2- light blue, EVI-3 purple), 75, 90, and 95 (green to yellow) percentile levels and fitted median-NDVI added in all plots for comparison (black line). The red absorption is the red surface reflectance – 1.0, i.e. what red down-welling solar flux that is not reflected is absorbed and drives photosynthesis. Values that are out of domain of EVI-3 are avoided by restricting the blue channel reflectance values less than 0.2 (blue<0.2).

When EVI-2 is plotted against EVI-3, the majority of the points fall close to the 1:1 line, indicating relatively good agreement between the two vegetation indices (Figure 3a). However, there is a second group of points for which EVI-3 has values that are significantly higher than those of EVI-2. A detailed inspection of the results spatially allowed us to identify the location of those pixels as being in regions covered by snow and ice, areas with sub-pixel clouds, and areas with haze, signaling artifacts in the EVI-3 index from non-vegetated sources as they were also reported in Vargas et al. (2013). The merging of EVI-3 and EVI-2 using EVI-2 in all problematic cases solved the issue.

When we compared the differences, globally and all periods, between the merging product and their components EVI-3 or EVI-2, we determined that the difference between the merged product and EVI-3 is insignificant (within ±0.02) in about 85% of the points, and the difference with EVI-2 is insignificant almost everywhere and every time (>99%) explaining more than 99% of the EVI merged product variance. Similar results were reported in Jiang et al. (2008).

When EVI-2 is plotted against NDVI, a tight relationship between both indices is observed (r^2 = 0.96, Figure 3b), and the problematic regions flagged by EVI-3 are not present. A curvilinear relation between NDVI and EVI-2 is a consequence of the greater dynamic range of NDVI as compared to EVI-2.

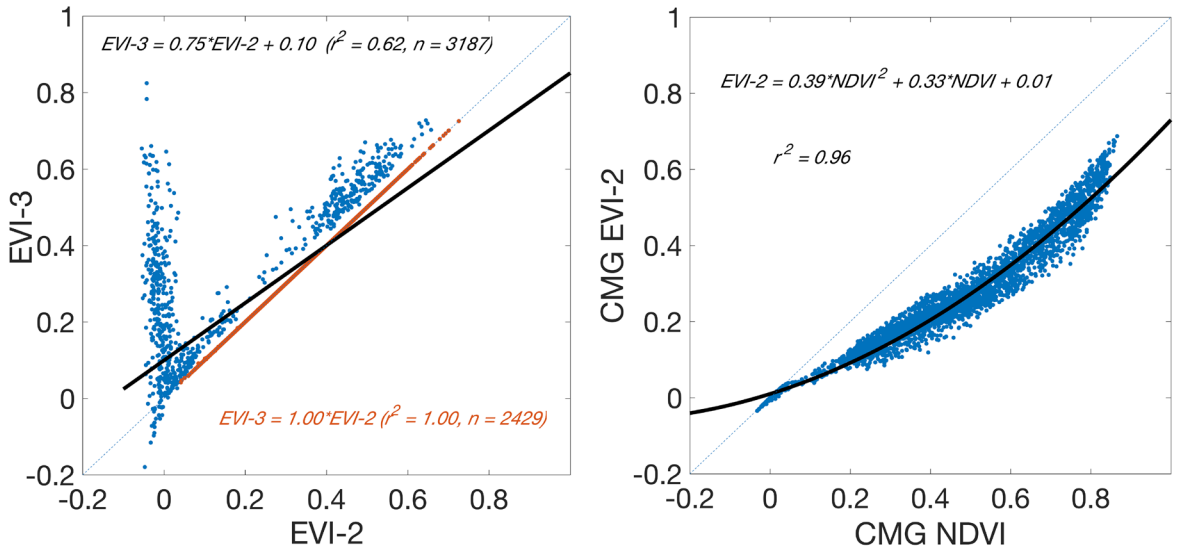

Figure 3. (a) SeaWIFS bi-monthly data comparing EVI-2 and EVI-3 data for 3,187 randomly selected from the 22 sample areas in (a) from 1998 to 2010. EVI-3 artifacts were identified as the cloud of blue points parallel to the Y axis and also above the red line. These are a manifestation of problems in the EVI-3 with snow, clouds, aerosols, and other atmospheric effects. When all points are included, EVI-3 data only explain 62% of the variance of the EVI merged product that uses EVI-2 in problematic case. When these EVI-3 artifacts are removed (cloud of blue points, about 24%), the remaining set of points (red points, about 76%), EVI-3 and the EVI-2 are perfectly correlated. In (b) we show MODIS climate modeling grid data comparing EVI-2 and NDVI for 1,832 points with a monthly time step. Note the curvilinear relationship between these two spectral vegetation indices which results from a greater dynamic range of NDVI than EVI-2.

VII.3.B. VEGETATION INDICES AND CHLOROPHYLL FLUORESCENCE RELATIONSHIPS

Our comparisons of the EVI-2 and NDVI using SeaWiFS bi-monthly data from 2007 to 2010 find them very similar with respect to GOME-2 SIF, with correlation values ranging between 0.92 and 0.94 (Figure 4). The proportion of explained variance is much higher than the one observed for the comparison between EVI-3 and SIF (r^2=0.74). In each case, we compared growing season integrals of SIF and the various vegetation indices. This approach could be used to inter-calibrate NDVI data with SIF data from GOME-2, to enable accurate annual estimates of gross primary production at 500 m for 2000 to 2016 with MODIS data and at 8 km from 1982 to 2016 with AVHRR data. The spatial resolution of the GOME-2 SIF data are 40 x 80 km. The greater variance of the EVI-3 data is a result of the atmospheric impacts explained above (as shown in Figure 3a).

Having determined that NDVI and EVI-2 are equally closely related to SIF, we next evaluated comparisons between MODIS CMG 5 km and GOME-2 SIF data (Figure 5). This analysis showed similar values of explained variance between NDVI and EVI-2 (r^2 values between 0.93 and 0.94).

We then investigated the NDVI-SIF relationship using 8-day time steps and 250 m MODIS data from 2007 to 2015 with the GOME-2 SIF data for the same 22 areas previously analyzed (Figure 6). We thus confirm similar NDVI-SIF relationships regardless of spatial resolutions and regardless of time steps.

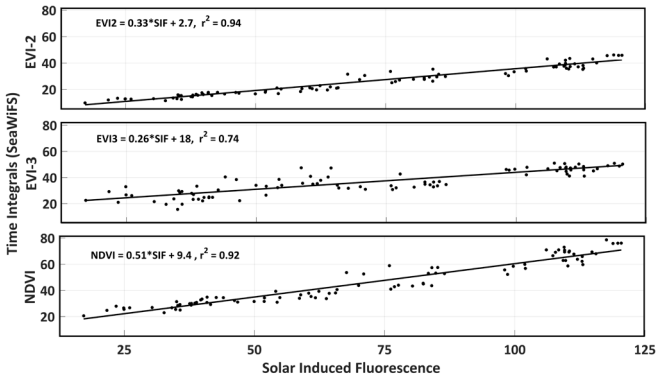

Figure 4. Time integrals of NDVI, EVI-3 and EVI-2 from SeaWiFS vs. Solar-induced chlorophyll fluorescence GOME-2 data for the 22 areas shown in figure 1. Bi-monthly time step data were used in this figure for 2007 to 2010.

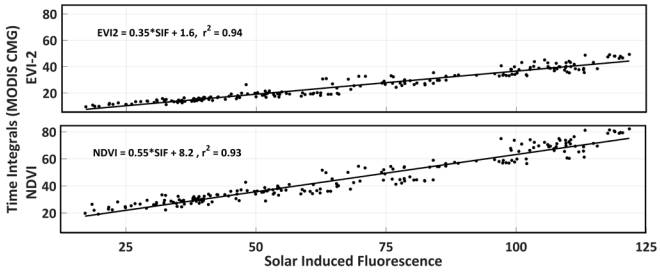

Figure 5. Time integrals of NDVI and EVI-2 from MODIS climate modeling grid 5 km data comparing EVI-2 and NDVI for 1,832 points to GOME-2 40 x 80 km SIF data for the twenty-two 200 x 200 km regions from 2007 to 2015 in figure 1. A monthly time step was used in this figure.

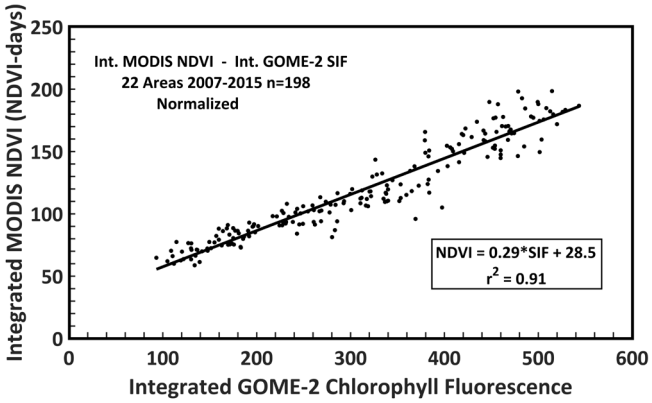

Figure 6. Comparison between eight-day 250 m MODIS NDVI data and 40 x 80 km GOME-2 SIF data for twenty-two 200 x 200 km regions in figure 1 from 2007 to 2015. Note the linear nature of this comparison that explains 91% of the variance between these variables.

VII.4. DISCUSSION

A problem with the EVI-3's formulation becomes apparent when it is plotted against other VIs (Figure 3a and Figure 4). The blue channel in the denominator of the EVI-3 formula has a negative coefficient, thus, any non-vegetation environmental influence that increases the blue channel is going to be multiplied by -7.5, artificially increasing the EVI-3 value. Aerosols, snow, sub-pixel clouds, and increased Rayleigh scattering all introduce artifacts into the EVI-3. For this reason, in standard MODIS processing, there is a list of tests to minimize this problem. When corrected, current MODIS processing replaces EVI-3 with EVI-2 using the so-called "backup algorithm" (Jiang et al. 2008). We found no improvement in the vegetation signal with the EVI-3 compared to the NDVI and EVI-2, no decoupling of the canopy background signal for the EVI-3, and no reduction in atmospheric influences with the EVI-3. In fact, we found the EVI-3 performs poorly when compared to the NDVI and the EVI-2 at all scales.

It has been proposed to discontinue the 3-channel EVI for VIIRS processing because of problems with the calibration of the blue band, making inter-calibration of 3-channel EVIs difficult among different instruments (i.e., blue surface reflectance from dense green vegetation is ~2-3% ±1-2%); problems with sub-pixel clouds, aerosols, and snow; the fact that MODIS data are atmospherically corrected; and the realization that the blue band is very highly correlated to the red band for vegetation in most vegetation settings. Another problem with the MODIS 3-channel EVI is that when problems with the MODIS blue band occur users cannot determine which vegetation index was used for the particular data they acquire, complicating attempts for consistent application. It is also impossible to calculate the 3-channel EVI from AVHRR data because there is no blue band for this instrument.

In addition to decisions on the choice of data sources and spectral indices, there are additional considerations of how to use them. Daily to bi-weekly data provide can be summed or integrated over growing seasons. While many options to make use of seasonal information are demonstrated in the studies reviewed by Yengoh et al. (2014), it is our opinion that a tremendous amount of information is present in NDVI or 2-channel EVI data through time. This has been substantiated by the vast number of peer-reviewed publications using AVHRR and MODIS time series data to study land vegetation (>7,500 as of March 12, 2017, from the Web of Science). A common approach using time series NDVI or EVI-2 data is to integrate these data over the growing season to determine GPP. We substantiate that approach through our use of solar-induced fluorescence that shows an almost 1:1 relationship between NDVI and solar-induced fluorescence and also between EVI-2 and solar-induced fluorescence (Figure 4 and Figure 5).

We found a direct linear relationship between solar-induced chlorophyll fluorescence measurements from the GOME-2 instrument and vegetation indices as surrogates for photosynthetic potential or capacity that enable accurate global to regional estimate of gross primary production at finer spatial resolution. Finally, we recommend NDVI as the vegetation index to monitor changes in productivity associated with land degradation as it is identical to the EVI-2 and has a wider dynamic range. We find a high degree of similarity and stability of red and near-infrared linear combinations, for both the NDVI and the EVI-2, substantiating the work of Tucker (1979) on red and near-infrared linear combinations.

VII. COMPARING NDVI TRENDS FROM DIFFERENT SENSORS AND SPATIAL SCALES

VIII. COMPARING NDVI TRENDS FROM DIFFERENT SENSORS AND SPATIAL SCALES

VIII.1. INTRODUCTION

The UNCCD distinguishes what to measure (indicators) from how it is assessed (metrics) as a means to understanding and reporting the status of degradation. In the context of LDN, the UNCCD has identified three land-based indicators and associated metrics: land cover, carbon stocks above and below ground, and land productivity or functioning of the land. Based on the results of the prior section, seasonal integrals of vegetation indices like NDVI can be used as indicators of change in vegetation productivity. In this section, we examine how trends calculated from time series of integrated NDVI, in four pilot countries, Senegal, Uganda, Kenya, and Tanzania, compare across sensors and across spatial scales.

It is important to note that achieving LDN requires considering all land changes whether due to human or natural causes (such as climate change). Quantifying the effect of climate variability on the NDVI signal is challenging (Yengoh et al. 2014). Previous studies analyzed linear trends of climate–adjusted integrated NDVI (∑NDVI) to avoid potential false alarms due to climate variability, such as drought cycles. A key tool is the trend of residuals (RESTREND) that adjusts ∑NDVI signals from the effect of particular climatic drivers. Most of the RESTREND studies (Wessels et al. 2007, Fensholt et al. 2013, Ibrahim et al. 2015) have used rainfall or soil moisture to identify the climate signal within NDVI using a pixel-by-pixel linear regression on NDVI time series and the climate signal (hereafter referred to as point-wise RESTREND in this report).

Point-wise RESTREND was found to be more effective at disentangling the effects of climate on the trends than the RUE method (Fensholt et al. 2011, Wessels et al. 2007) and thus suggested as a better indicator of land degradation. However, Wessels et al. (2012) and Fensholt et al. (2013) found that the assumption of a strong linearity between rainfall and NDVI used in point-wise RESTREND has in fact shortcomings in semi-arid regions. Although some pixels might have a theoretical justification for assuming a linear model relating climate and ∑NDVI, the assumption of a linear relationship can add complication to the interpretation of point-wise RESTREND results. In fact, implicit in the point-wise approach is that the linear functionality varies from pixel to pixel (due to variation in, for example, ecosystem type) and that the coefficients of the model accurately represent the uncertainty expected within or among ecosystems. However, this uncertainty is intertwined with other non-climate sources of variability that makes their interpretation more difficult.

Fensholt et al. (2013) obtain meaningful results from a RUE temporal trend analysis by restricting the analysis in the Sahel only to pixels for which linearity is shown to exist (only 37% satisfy these requirements). These limitations point, in fact, to a shortcoming of a point-wise (regression) approach when trying to capture the functionality between variables within and among ecosystems. Point-wise RESTREND blindly tries to adjust and explain most of the variance – even variance that is better explain from unrelated variables (e.g. impacts of soil types, altitude ranges, land-cover types). Thus, the interpretation of a point-wise RESTREND analysis as a climate independent metric is not as straight forward as users of climate data might reasonably assume (Koster et al. 2009), since the uncertainties of the screened NDVI integration themselves and the differences in the point-wise approximations, from pixel to pixel, become entangled.

A convenient simplification that enables us to describe large-scale patterns of the effects of precipitation or soil moisture on vegetation processes is to look at soil moisture- or precipitation-vegetation relationships as a global transfer functional within a terrestrial ecosystem (Sellers 1987). That is, a function that transforms climate variability into the vegetation domain leaving out potential vegetation variance explained by other non-climate variables. This simplification should facilitate interpretation of (large-scale) patterns that provide an average description of the general expected effects from climate within the ecosystem. Vegetation-variance observed and accounted for by multiple non-climate effects is expected to propagate as uncertainty into the functional. As we explain in the next section, to describe the average response of vegetation to precipitation or soil moisture variability, we compute their joint probability density function and fit a unique non-linear (system) function to the median profile of the response. Thus, we propose a system RESTREND as opposed to the point-wise RESTREND approach to examine how NDVI trends vary over space and across sensors and spatial scales when the effects of climate are removed according to a common baseline global transfer functional.

VIII.2. ANALYTICAL METHODS

Using data from two sensors (MODIS and AVHRR), we compute seasonal integrals of NDVI for each of the four pilot countries: Kenya, Tanzania, Uganda, and Senegal. We then compare the trends of the integrated NDVI with the residual trends after removing the effects of soil moisture and precipitation.

VIII.2.A. NDVI TREND ANALYSIS

First, we calculate the seasonal NDVI climatology (NDVIs) at pixel-level and at each composite period (15-day or monthly), defined as the mean value of the NDVI within the composite period using the entire 34-year AVHRR NDVI record. Climatology NDVIs is computed using only good quality NDVI observations within each year. Second, we calculate the integrated growing season NDVI ($\sum_{gs}$ NDVI) for each pixel and each year. Third, trends are estimated from the slopes of linear regressions over the yearly $\sum_{gs}$NDVI integrals. Here, growing season is defined at pixel-level as periods during a year where NDVI is greater than 0.1 (NDVI>0.1). The growing season could be dynamic when based on individual years (NDVI>0.1) or static when based on the NDVI climatology (NDVIs>0.1). Both methods were compared, and no significant differences were found in the resulting NDVI trends. The results presented in this report are based on the static definition, since it allows us to define a common baseline, calculating the growing season integrals as the mean NDVI values over the same growing period for all the years.

Once the growing season periods are identified, we calculate time series of $\sum_{gs}$ NDVI for 250 m MODIS MOD09Q1, 5 km MODIS Climate Modeling Grid (CMG), and 8 km NDVI3g data (Table 4) and repeat the process to estimate trends for each dataset. To allow comparisons among the slopes of $\sum_{gs}$ NDVI datasets at a common spatial scale, we converted the two MODIS-derived datasets to the 8 km NDVI3g grid. We converted the 250 m MODIS data to that grid by calculating mean NDVI within each 8 km NDVI3g pixel. We converted the 5 km CMG to the 8 km NDVI3g grid using a nearest-neighbor resampling. In the current study, we focused on AVHRR-NDVI3g and MODIS-derived indices given their favorable comparison to alternative datasets, and the longer instrumental records they provide.

VIII.2.B. NDVI RESIDUAL TREND ANALYSIS

We test both soil moisture and precipitation datasets for quantifying the effects of climate on NDVI.

There are a number of operational soil moisture products. This study uses the 0.5° by 0.625° "Modern-Era Retrospective analysis for Research and Applications version 2 (MERRA-2) root zone soil moisture at a fixed layer thickness of 1 m product (Bosilovich et al. 2015).

Data Source	Spatial Resolution(s)	Temporal Resolution(s)	Use
MODIS MOD09Q1 collection 6	250 km	8-day composite	Calculation of trends of integrated NDVI over the growing season from RED and NIR channels from data from the Aqua satellite for 2003 to 2015.
MODIS CMG	5 km	16-day composite	Calculation of trends of integrated NDVI over the growing season from RED and NIR channels from 2003 to 2015 data.
AVHRR NDVI3g	8 km	Bi-monthly composite	Calculation of growing season start and end dates from 1982-2015 data, and calculation of trends of integrated NDVI over the growing season from RED and NIR channels from 2003 to 2015 data.

Table 4. List of vegetation index datasets used in this analysis.

The MERRA-2 atmospheric reanalysis provides global, hourly estimates of different land conditions, among them root zone soil moisture, 2-meter air temperature, humidity and many others. NASA's Global Modeling and Assimilation Office (GMAO) conducted an evaluation of the different MERRA-2 products (Reichle et al. 2016), in particular, improved 2-meter air temperature and humidity by comparing corresponding records with 5° by 5° land surface Hadley Center's HadISDH humidity and temperature data and the ERA-Interim (ERA-I) 0.75° by 0.75° equivalent temperature and humidity products (Balsamo et al. 2015). Biases were observed in MERRA-2 for boreal areas only, with MERRA-2 showing good agreement with ERA-I everywhere else. ERA-I shows good agreement to the Hadley Center's HadISDH data even in Boreal areas, suggesting that the discrepancies in northern Eurasia are due to known MERRA-2 biases.

The validation of MERRA-2 surface and root zone soil moisture was done using in situ measurements from a number of sites representing a robust variety of climatological conditions. The Reichle et al. (2016) study also compared the skill of MERRA-2 and ERA-I/Land, which uses an updated land surface model and meteorological forcing corrected with monthly global precipitation, since precipitation is the dominant variable of land surface hydrological conditions (Bosilovich et al. 2015). The results are very similar to the comparison with ERA-I, but with MERRA-2 showing slightly higher surface and root zone soil moisture accuracies than ERA-I/Land (Reichle et al. 2016). Since MERRA-2 is based on daily data compared to monthly ERA-I data, it is not surprising that MERRA-2 appears to be a better data set for soil moisture than the ERA-I soil moisture data.

The NOAA National Centers for Environment Prediction (NCEP) provides a 0.5° by 0.5° gridded soil moisture product (van den Dool et al. 2003); however, MERRA-2 soil moisture products are improved significantly from NOAA's NCEP soil moisture dataset due to an updated land surface model and meteorological forcing from daily satellite data assimilation. NCEP has not been upgraded since 2003 and still uses a one-layer hydrological model compared to a significantly more sophisticated coupled atmosphere-land modeling system in MERRA-2 or ERA-I.

We also test removal of climate effects using precipitation. We use the Global Precipitation Climatology Project (GPCP) version 2.3 2.5° x 2.5° dataset, which blends station records, satellite, and sounding observations to estimate monthly rainfall from 1979 to the present.

Data Source	Spatial Resolution(s)	Temporal Resolution(s)	Use
MODIS MOD09Q1 collection 6	250 km	8-day composite	Calculation of trends of integrated NDVI over the growing season from RED and NIR channels from data from the Aqua satellite for 2003 to 2015.
MODIS CMG	5 km	16-day composite	Calculation of residual trends of integrated NDVI over the growing season after removal of climate effects using soil moisture or precipitation. NDVI was calculated from RED and NIR channels from 2003-2015 data.
AVHRR NDVI3g	8 km	Bi-monthly composite	Calculation of growing season start and end dates from 1982-2015 data, and calculation of trends of integrated NDVI over the growing season from RED and NIR channels from 2003-2015 data.
MERRA-2 Soil moisture	0.5° by 0.625°	daily	Used to predict NDVI for estimation of residual trends derived from monthly and yearly data.
GPCP precipitation	2.5° by 2.5°	monthly	Calculation of total monthly precipitation for use in predicting a monthly and yearly integrated NDVI data.

Table 5. List of datasets used in residual trend analysis.

The point-wise RESTREND approach attempts to remove the effects of climate on the $\sum_{gs}$ NDVI integrals to allow identification of trends that are independent of variations in climate. To compute residual trends, first the vegetation index time series must be integrated over the growing season.

In the point-wise RESTREND, a regression is then performed at the pixel level that predicts the NDVI signal on the basis of a climate indicator, such as soil moisture or precipitation. A second regression is then performed on the residuals from this first regression, to map trends in the signal that remain once the effects of the climate indicator are removed.

While recognizing that vegetation responds to climate and to other non-climate related effects (e.g. effects of land cover types, altitude ranges, soil types) in many different ways and in a non-linear fashion, we build a system-wise RESTREND to capture and describe large-scale patterns of the climate effects by looking at soil moisture- or precipitation-vegetation relationships as a global transfer functional within a terrestrial ecosystem. To build the functional for the system-wise RESTREND (hereafter referred to as system RESTREND), we first compute the joint probability density function (pdf) between the climate variable (precipitation or soil moisture) and the vegetation variable (NDVI) using more than four million random points taken from the four countries, and also from tropical dry-sub-humid or semi-arid areas elsewhere in the Sahel. Then, the system functional is derived from curve fitting of the median value of the pdf.

The contributions from other effects, e.g. land cover types and soil types are described as uncertainties at each climate value of the system functional. Once the global functional is defined, we compute predicted $\sum_{gs}$ NDVI integrals, i.e. growing season integrals of predicted-NDVI from each precipitation and soil moisture functional. We then compare predicted $\sum_{gs}$ NDVI with observed $\sum_{gs}$ NDVI integrals to calculate the residuals, and examine the trends in these residuals (slopes of linear regressions on the residuals). We map these system RESTREND trends using both the soil moisture and precipitation to identify areas where NDVI is increasing or decreasing independent of the climate signal, and then compare variation in the results dependent on the chosen climate dataset (Figure A.5).

VIII.3. RESULTS

We develop relationships from the joint pdfs between soil moisture and NDVI and precipitation and NDVI both globally (Figure 7) and for each of the four countries (Figure A.4). A piecewise polynomial (system functional F_s, Table 6 and black line in Figure 7, left) was therefore fit to the median profile of the global joint soil-vegetation pdf (orange line in Figure 7, left) explaining almost all variance of the median profile. The functional F_s and the median profile shows a distinct breakpoint around 0.35 m3 m-3, indicating that, after soil moisture reaches this critical value, vegetation rapidly responds. In fact, F_s structure is consistent to the expected response of plant-water potential to soil moisture (Gardner 1983, Sellers 1997). Under moist-soil conditions (soil moisture $m^3\ m^{-3}$ > 0.39 in Table 6), vegetation structure and surface roughness effects control much more strongly the rate of water loss through evapotranspiration (Gardner 1983, Sellers 1997). As soil moisture declines (0.37 < soil moisture < 0.39), the control over evapotranspiration shifts from canopy structure to soil moisture and as soils continue to dry, however, their hydraulic conductivity declines and this creates a relatively abrupt threshold of soil moisture (soil moisture < 0.37), below which the rate of water supply to roots declines, and plants experience water stress or they wilt because they cannot obtain water from soils (Gardner 1983). The absolute values of the breakpoints are strongly model-specific, essentially, they are an index of MERRA-2 moisture state (Koster 2009). However, similar structures are expected from ERA-I soil moisture data since the information content of soil moisture data lies mostly in the time variability that is mutually consistent between the different soil moisture products (Koster 2009).

The global joint precipitation-vegetation pdf (Figure 7, right) shows a smoother response of vegetation to precipitation. Notice that the functional F_p (Table 6 and black line in Figure 7, right) is relatively insensitive to high precipitation amounts (precipitation > 5 mm/day). In fact, under these conditions evapotranspiration varies little whereas runoff is quite sensitive to the quantity of precipitation (Bormann and Likens 1979). The uncertainty of the functional F_p appears to be explained by runoff within these precipitation ranges. Notice also the quasi-linearity of F_p for moderate to low precipitation amounts (precipitation < 5 mm/day) but still high uncertainty. These correspond to dry canopies where evapotranspiration is relatively insensitive to precipitation over a broad range of soil moisture (Bormann and Likens 1979). This quasi-linearity of F_p might well explain the meaning results of Fensholt et al. (2013) using RUE and point-wise RESTREND trend analysis after restricting it to pixels for which linearity is shown to exist in the Sahel.

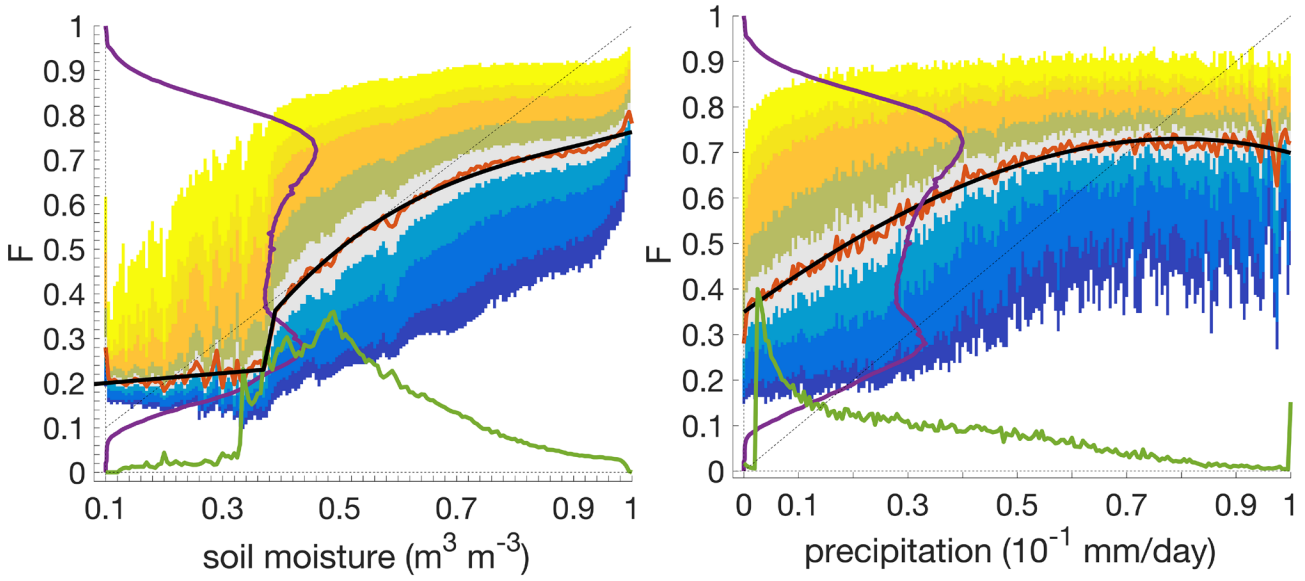

Figure 7. Relationship between soil moisture and NDVI, and between precipitation and NDVI used to predict NDVI in the RESTREND procedure. This figure plots soil moisture versus NDVI (left) and precipitation versus NDVI (right) for a set of random points selected from global AVHRR NDVI3g data from 1982-2015. The colorbars indicate quantiles from highest (yellow) to lowest (blue) values as follows (light yellow = 95%-100%, dark yellow = 90%-95%, orange = 75%-90%, green = 60%-75%, gray = 40%-60%, light blue = 25%-40%, blue = 10%-25%, and dark blue = 5%-10%). The purple line on the left of each plot is the distribution of the NDVI data. The green line on the bottom is the distribution of the particular climate dataset (soil moisture on the left, precipitation the right). The orange line is the median profile. The black line is the functional fit to the median profile of the joint pdfs (piecewise on the left, a third-degree polynomial on the right, as noted in Table 5).

Climate Indicator	Interval	Equation
Soil Moisture (functional F_s)	$0.10 \leq x < 0.37$	$0.11x + 0.19$
	$0.37 \leq x < 0.39$	$6.63x - 2.22$
	$0.39 \leq x < 1$	$1.38x^3 - 3.81x^2 + 3.83x - 0.63$
Precipitation (F_p)	$0 \leq x < 1$	$-0.14x^3 - 0.38x^2 + 0.87x + 0.35$

Table 6. Regression equations used to fit the observed global relationships between soil moisture and NDVI, and between precipitation and NDVI. Note that the soil moisture-NDVI relationship was modeled with a piecewise regression, while the precipitation-NDVI relationship was modeled with a third-degree polynomial.

We study the effects of lags and yearly integration when applied to each functional to study the variability of the relationships (see Figure A.2 in appendix). Soil moisture functional seems to be invariant to lag and integration (Figure A.2a, b), a consequence that reflects the invariance of water movement from soil to the roots of transpiring plants (Sellers et al. 1997): water moves along the gradient from high to low potential energy; plants can extract water from soil depending on soil field capacity; as soil dries, hydraulic conductivity declines, and the root accesses water less rapidly as soil holds the remaining water more tightly (Sellers 1987), This is not the case for precipitation where lags and integrated functional differ from each other (Figure A.2c,d). This is expected since precipitation has components that do not directly affect vegetation, e.g. runoff, but that could have effects on the relationship. However, the relationship between integrated precipitation and NDVI appears to attenuate the potential runoff contributions to the uncertainty of the functional F_p (Figure A.2d).

To test whether the response of vegetation to soil moisture and to precipitation in each of the four pilot countries follows the global pattern we plotted these relationships individually for each country (Figure A.4). The vegetation response to soil moisture and precipitation is unique in each of the four pilot countries. Vegetation in Senegal shows the slowest response to increasing soil moisture, while vegetation in Uganda rapidly greens after a threshold of 0.35 m^3 H20 m^{-3} soil. Vegetation in Kenya greens in a linear fashion with increasing soil moisture after a threshold of 0.35 m^3 H20 m^{-3} soil. Vegetation in Tanzania shows a similar response, though with a slower green up at low levels of soil moisture. In general, the response of vegetation to precipitation is similar in Senegal and Kenya with a monotonic relationship between precipitation increase and NDVI. Vegetation in Uganda and Tanzania has a similar response to precipitation increase, though different from the pattern in Senegal and Kenya. This difference is expected since those countries have different land-covers and therefore different NDVI variability which is clear from the distribution of vegetation values. That is another way to emphasize the importance of capturing the robust functionality between vegetation and transpiration dependencies, using NDVI and soil moisture.

Using the global relationships derived in Figure 7, we calculated the system RESTREND for Senegal (Figure 8), Tanzania, Uganda, and Kenya (Figure 9). For comparison, we also calculated the NDVI integral trends for each of the four countries (Figure 10). We also computed the point-wise RESTREND for the same time period and datasets, to assess the effect of the two different RESTREND methods on the NDVI trends identified for the four pilot countries (Figure A.5). The NDVI trend and the P-RESTREND method (both using soil moisture and precipitation), show similar trends, indicating that the point-wise RESTREND method is not really able to remove the climate signal from the overall plant productivity trend captured by raw NDVI. However, the system RESTREND method is able to highlight trends that differ from those of NDVI, indicating a potential contribution to the removal of the climatic effect from raw NDVI data.

In Senegal, the NDVI trends, P-RESTREND (both rainfall and soil moisture) and precipitation S-RESTREND, show increases in NDVI across most the country. The soil moisture S-RESTREND analysis however, shows declines east of Dakar that do not appear in the other analysis. In Kenya, the soil moisture S-RESTREND analysis identifies decreases in NDVI in the NW part of the country, which differ from the trends depicted by NDVI trends and P-RESTREND. In Uganda, the soil moisture S-RESTREND analysis shows strong increases in NDVI in northern Uganda – these increases are weaker and less consistent spatially in the other results. Tanzania similarly shows regions with different patterns of change between the NDVI trend, S-RESTREND and P-RESTREND results. The largest difference is that soil moisture S-RESTREND results show large and significant declines in NDVI in central and southeastern Tanzania whereas the other products show increases or minor decreases in those areas.

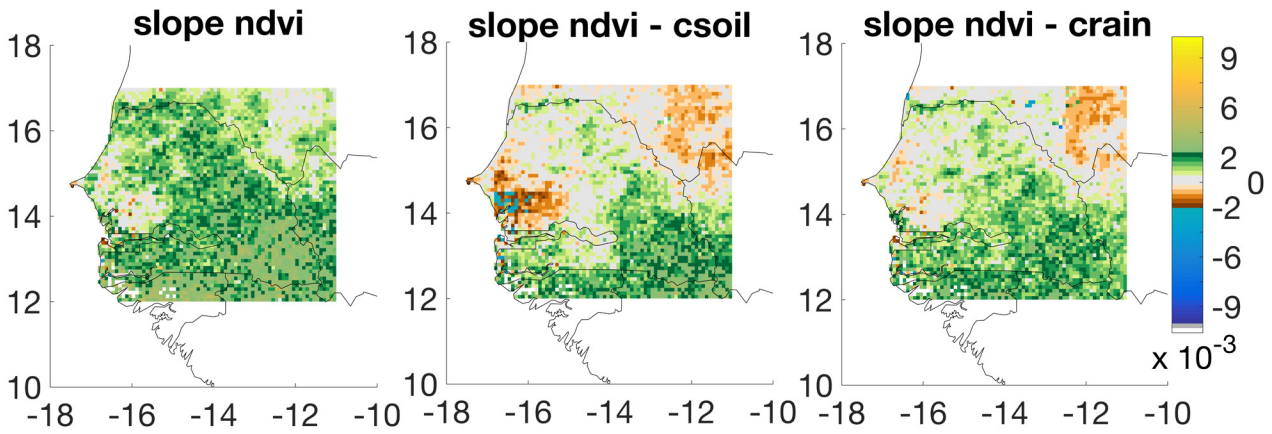

Figure 8. Senegal system RESTREND results from 1982-2015 GIMMS3g NDVI data using soil moisture and rainfall as climate estimators. Note the unevenly distributed color ramp for better illustration of the variability around zero. The rapid transition in color between -0.002 and 0, and between 0 and 0.002 is to account for the sensitivity to inter-annual variation (trends) of the NDVI dataset (Pinzon and Tucker 2014). The detectability of inter-annual variations increases proportional to NDVI values and it ranges from the lowest 0.0012 (at dry areas) to 0.012 (at forested areas). Slopes within the range of ±0.0012 are not differentiable from noise uncertainty, and therefore cannot be definitively used to indicate change even if the slope is significant (gray area). Results are smoothed over a 32 km x 32 km window to highlight aggregations of land productivity increasing or decreasing.

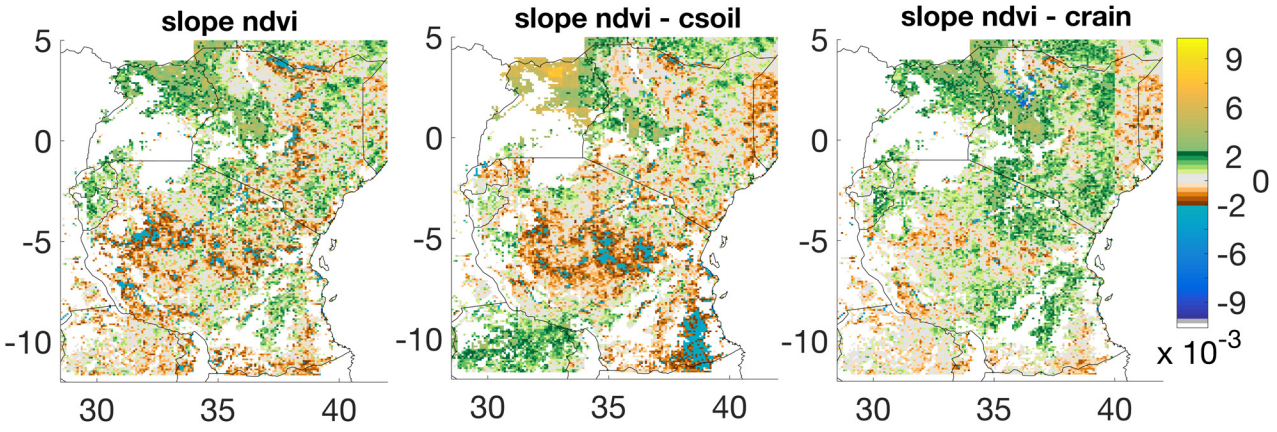

Figure 9. Kenya, Uganda, and Tanzania system RESTREND results from 1982-2015 GIMMS3g NDVI data using soil moisture and rainfall as climate estimators. Note the unevenly distributed color ramp for better illustration of the variability around zero. The rapid transition in color between -0.002 and 0, and between 0 and 0.002 is to account for the sensitivity to inter-annual variation (trends) of the NDVI dataset (Pinzon and Tucker 2014). The detectability of inter-annual variations increases proportional to NDVI values and it ranges from the lowest 0.0012 (at dry areas) to 0.012 (at forested areas). Slopes within the range of ±0.0012 are not differentiable from noise uncertainty, and therefore cannot be definitively used to indicate change even if the slope is significant (gray area). Results are smoothed over a 32 km x 32 km window to highlight aggregations of degradation or improvement.

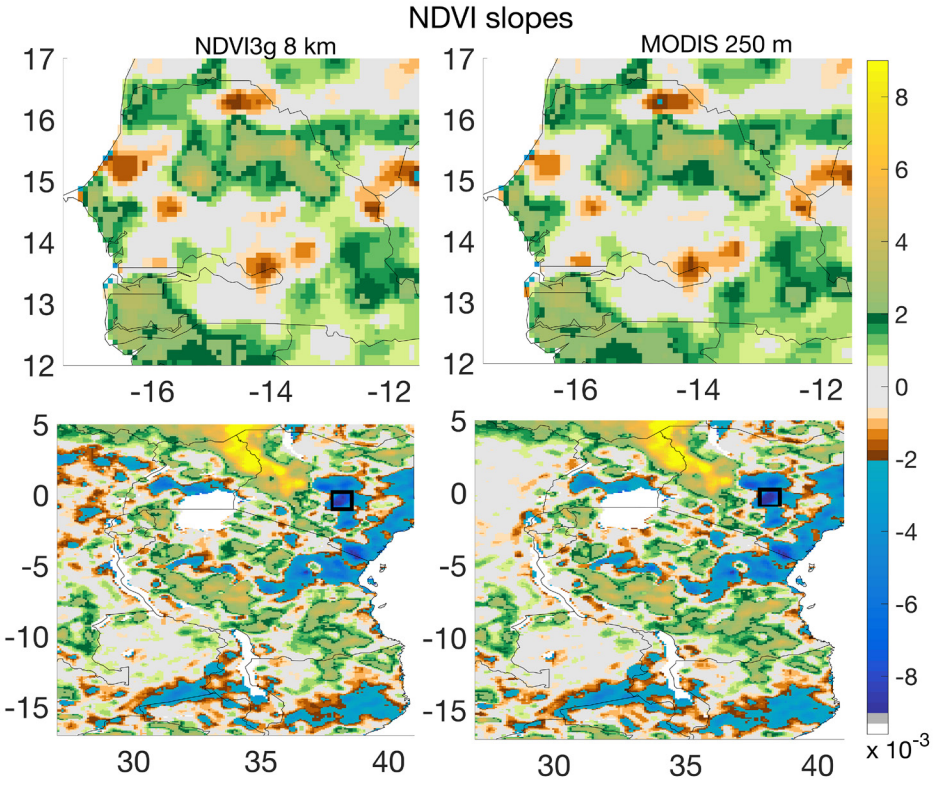

Figure 10. Comparison of NDVI annual integral slopes from 2003-2015 GIMMS3g NDVI data (left side) and from 2003-2015 MODIS NDVI data (right side) as predictors of land degradation. See Figure 11 for the plotted data from the rectangle in the lower right hand image. Results are smoothed over a 32 km x 32 km window to highlight aggregations of degradation or improvement.

To demonstrate how the soil moisture-based and precipitation-based RESTREND results compare, we plot the time series of residuals for an area in northern Kenya, centered at 1° N and 38° E (Figure 11). Though the mean value of the RESTREND varies between the two series, both time series show similar long term trends.

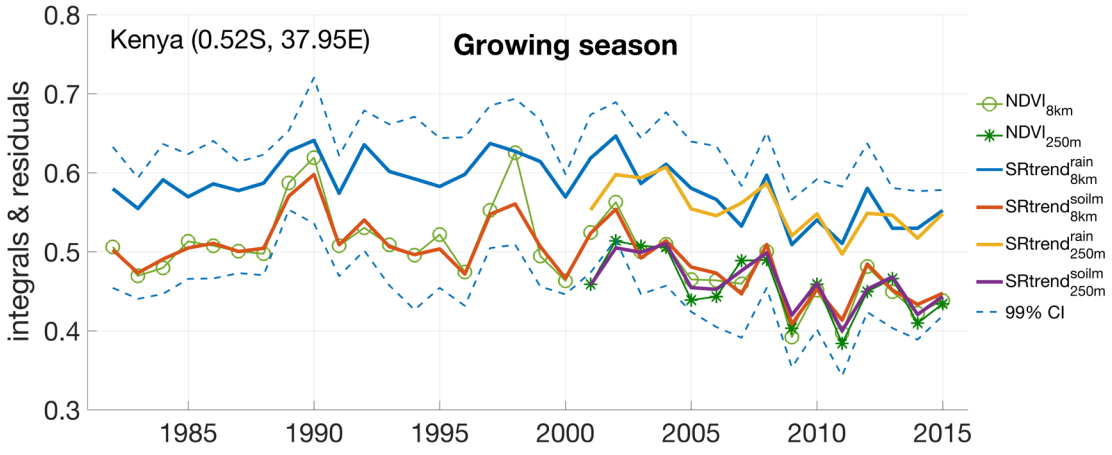

Figure 11. Time series of Integrals and mean residuals from S-RESTREND analysis for an area in Kenya centered at 0.52°South latitude and 37.95°East longitude with a radius of 15 km. This plot shows results from both the 8 km NDVI3g dataset (1982-2015) and the 250 m MODIS dataset (2001-2015), and for each dataset shows results from both the soil moisture and rainfall-based S-RESTREND analyses. Note the similarities and the negative trends in the data sources from 2001 to 2015, the time period covered by both the NDVI3g and MODIS data.

We also compare the integrals of predicted NDVI using soil moisture at monthly (f_m(soil)) and annual integrals (f_a(soil)) (Figure A.3a). The consistency and robustness of the functional is apparent in the one-to-one relationship between f_m(soil) and f_a(soil) even though they generate different probability density functions (green and purple lines). As expected, the predicted NDVI from annual integrals by f_a(soil) (x-axis) is smoother than the predictions from monthly soil data (f_m(soil)) (y-axis), and the functional appears to be invariant. Notice that this consistency is corroborated by the comparison of the residuals of NDVI using soil moisture at monthly (f_{sm}) and annual levels (f_{sa}) (Figure A.3b). The Gaussian-tendency of the probability density functions show the variability of vegetation is dominated and captured by the soil moisture as a climate variable.

The Gaussian-like pdfs in (Figure A.3b) play as catalysts for a better understanding of the properties of the functionals f_s and f_p in the S-RESTREND analysis. We start by centering $NDVI_s$ = f_s(soil) and $NDVI_p$ = f_p(precipitation) around the long-term average of NDVI at each pixel, that is,

$$NDVI_s^c(\mathrm{x}) = f_s\left(\mathrm{soil(x)}\right) - \mathrm{avg}\left(f_s\left(\mathrm{soil(x)}\right)\right) + \mathrm{avg(NDVI(x))} \qquad (4a)$$

$$NDVI_p^c(\mathrm{x}) = f_p\left(\mathrm{rain(x)}\right) - \mathrm{avg}\left(f_p\left(\mathrm{rain(x)}\right)\right) + \mathrm{avg(NDVI(x))}) \qquad (4b)$$

We then computed their joint pdfs (Figure 12). They all converge into one-to-one line. Reordering terms in equations (4a) and (4b), and given that NDVI(x) $\approx NDVI_s^c(\mathrm{x}) \approx NDVI_p^c(\mathrm{x})$ from Figure 12,

$$\mathrm{NDVI(x)} \approx NDVI_s^c(\mathrm{x}) = f_s\left(\mathrm{soil(x)}\right) - \mathrm{avg}\left(f_s\left(\mathrm{soil(x)}\right)\right) + \mathrm{avg(NDVI(x))}$$

$$\mathrm{NDVI(x)} - \mathrm{avg(NDVI(x))} \approx f_s\left(\mathrm{soil(x)}\right) - \mathrm{avg}\left(f_s\left(\mathrm{soil(x)}\right)\right) \text{ and} \qquad (5a)$$

$$\mathrm{NDVI(x)} - \mathrm{avg(NDVI(x))} \approx f_p\left(\mathrm{rain(x)}\right) - \mathrm{avg}\left(f_p\left(\mathrm{rain(x)}\right)\right) \qquad (5b)$$

In other words, Equations (5a) and (5b), confirmed that climate variability (by soil moisture or precipitation) governs vegetation (NDVI) variability. But what it is more important is that by explaining most of the vegetation variability we derive to a more precise functionality,

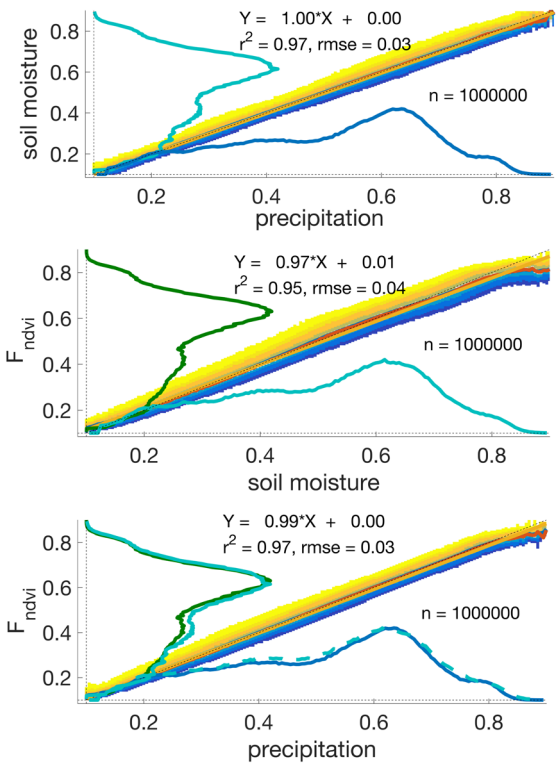

Figure 12. Joint probability density functions for NDVI (F_{ndvi}), centered NDVIs = F_s(soil) (soil moisture), and centered $NDVI_p$ = F_p(rain) (precipitation). They all converge into one-to-one lines.

In other words, the variance unexplained by the original functional F_s is carried out, at most of the pixels, by the long-term NDVI average – a key component of land cover discrimination. And it is static. The S-RESTREND allows us to interpret these dependencies much better and facilitates interpretations through Equation (6).

$$\mathrm{NDVI(x)} \approx f_s\left(\mathrm{soil(x)}\right) - \mathrm{avg}\left(f_s\left(\mathrm{soil(x)}\right)\right) + \mathrm{avg(NDVI(x))}$$

$$\approx f_p\left(\mathrm{rain(x)}\right) - \mathrm{avg}\left(f_p\left(\mathrm{rain(x)}\right)\right) + \mathrm{avg(NDVI(x))} \qquad (6)$$

VIII.4. DISCUSSION

The NDVI trends identified from 8 km AVHRR NDVI3g and 5 km MODIS CMG largely correspond to each other. When the trends are compared with those identified by aggregating 250 m MODIS data to 8 km, the patterns show great homogeneity among the sensors and datasets. Our results thus "scale", which means these relationships are independent of specific spatial resolutions. The S-RESTREND approach of NDVI using MERRA-2 soil moisture provides a much more robust and consistent identification of areas that show decreases in primary productivity than using rainfall (Figure A.5). In particular, the S-RESTREND analysis in Senegal (Figure 8) provides evidence that the NDVI greening or positive trends of growing season integrals of NDVI were correct. Fensholt et al. (2012) cautioned about the direct interpretation of the recovery of vegetation, since they might have widely different explanations. In fact, recent studies relating long-term NDVI ground observations in Senegal show positive NDVI trends when vegetation replacement occurred (Herrmann and Tappan 2013, Brandt et al. 2016). When S-RESTREND is applied to NDVI integrals using soil moisture, some of the regions with positive trends reversed sign and showed decreases in primary productivity (negative RESTREND trends) around the regions where Herrmann and Tappan (2013) showed impoverishment. This result does not, however, provide a validation of the S-RESTREND results, since such analysis allows only certain causes to be inferred. In fact, S-RESTREND analysis can only give indications of causal relationships when combined with information on growth constrains (impoverishment of woody vegetation cover). Still, S-RESTREND at least provides the catalyst for searching causal hypothesis and their potential testing where other sources are available, e.g. ground data, high-resolution imagery. Moreover, S-RESTREND facilitates interpretation since the variance unexplained by the original functional F_s is carried, at most of the pixels, by the long-term NDVI average which is a key component of land cover discrimination.

Atuherie Shallon and Tomusherure Kofudance cook potatoes at the family's farm along a park boundary in Uganda.

IX. NEXT STEPS: INTEGRATING LAND COVER CHANGE INTO LAND DEGRADATION MONITORING AT MULTIPLE SCALES

IX. NEXT STEPS: INTEGRATING LAND COVER CHANGE INTO LAND DEGRADATION MONITORING AT MULTIPLE SCALES

IX.1. INTRODUCTION

NDVI datasets at 250 m to 8 km are useful to study land degradation, although they lack the detail to reveal the kind of degradation or the drivers (Bai et al. 2008a). Other datasets, such as very high resolution commercial imagery, offer potential to investigate the types and drivers of land degradation once degradation trends are identified using NDVI. When RESTREND results from coarse-resolution MODIS 250 m data are combined with moderate to high-resolution sensors, such as 30 m Landsat, 30 m Aster, 20 m Sentinel-2a and Sentinel-2b, and 30-50 cm commercial data, one can obtain enough spatial and spectral detail to discriminate changes among individual trees and to interpret the kind of degradation or drivers (Table 7).

ESA's Sentinel-2a and Sentinel-2b, both with a 20 m spatial resolution, and Landsat-8's 30 m products are the most widely accessible medium-to-high spatial resolution multispectral satellite data. The potential for synergistic use of the two sources creates opportunities for timely and accurate observation of Earth status and dynamics at the 30-m scale. In addition, incorporation of 30-50 cm commercial satellite data is of fundamental importance for the scientific community for the accurate interpretation of land degradation and for identification of drivers (Masek et al. 2016). In this section, we outline an approach to interpret degradation and drivers using high-resolution commercial satellite data.

IX.2. PROPOSED ANALYTICAL METHODS

Monitoring patch-scale vegetation dynamics, particularly for degraded and agricultural regions, requires both fine spatial resolution and an 8-day temporal frequency. While this is a very difficult task for a single moderate to high-resolution sensor, harmonizing multiple international sources of data can provide a cost-effective pathway to such a capability. NASA, the USGS, and ESA have started a collaboration to develop a processing chain that creates seamless, "harmonized" reflectance products from combined Landsat, Sentinel-2a, and Sentinel-2b observations. The "harmonization" approach uses standardized atmospheric correction, BRDF adjustment, spectral band-pass adjustment, and gridding algorithms to guarantee same geophysical measurements, taking advantage that both sensors are similar in terms of spectral and spatial measurements.

These products point the way to a "30-m MODIS" capability for agricultural, ecosystem monitoring and land degradation monitoring by leveraging international sensors. When combined, observations from both sensors can provide 2-4 day coverage for global land areas (Masek et al. 2016). Data are processed on NASA Earth Exchange cluster at NASA Ames from automated pulling and download of ESA SciHub and USGS Earth Explorer for input files. Although during the first year of activity these data have been produced over a limited number of sites, our land degradation team has accessed these "harmonized" data from Senegal and Tanzania for our analysis.

The opening of free USGS Landsat archive in 2008 ushered in a new era of applications and wider uses of Landsat data. More accurate and reliable spatial analysis over large areas resulted and improved the quality of decisions based on these data. Since then, the new focus has been on leveraging the time domain for inter-annual disturbance, land degradation, land use, and vegetation gross primary production.

The capability of Sustained Land Imaging from Landsat-8, Sentinel-2a, and Sentinel-2b provides a unique opportunity to track land changes. We use the time domain to analyze moderate-resolution imagery as we have for years with AVHRR, MODIS and other ~1 km systems. Moving from single test site to continental data is a big challenge, and the combination of coarse-resolution data with more detail provided by Sustained Land Imaging will be valuable. During 2016, "harmonized" Landsat-8 and Sentinel-2a data were produced over a limited number of locations, including Senegal and Tanzania. High spatial resolution commercial satellite data will also complement "harmonized" Landsat-8 and Sentinel-2 data.

Another indicator of land degradation is change in land cover or change in land use. To investigate land degradation from change in land cover or change in land use, we used Digital Globe WorldView-2 satellite data for the area identified as being degraded land in Figure 13 in Kenya. We found the degraded area had been converted from natural vegetation to agricultural land.

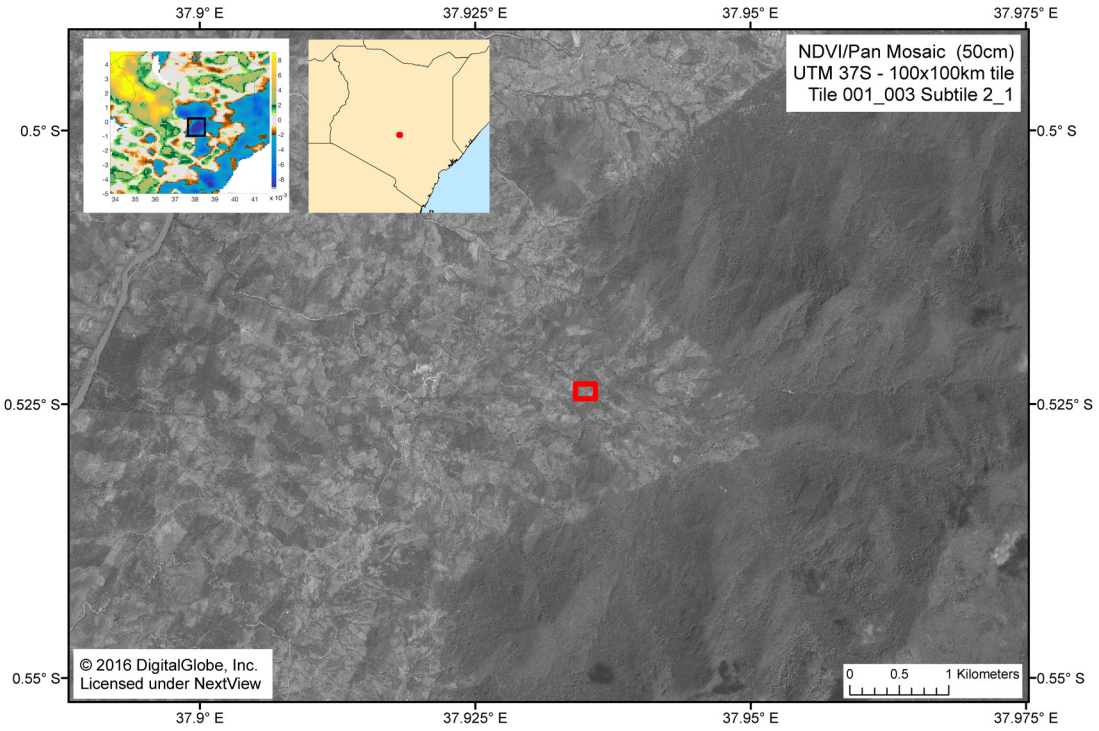

Figure 13. An example of a 50 cm commercial satellite data mosaic for one of the areas in Kenya where we decreases in primary productivity in Figure 9. The altered land appears on the left side of this figure, where natural vegetation on the right has been converted to farm land. A full-resolution 50 cm subset of this appears in the appendix as Figure A.15.

We are producing commercial satellite data mosaics for all of Senegal, Uganda, Kenya and Tanzania for use in detailed land cover and land use mapping with Landsat-8 and Sentinel-2a data (Figure 14). These detailed data have never been used previously at this large a spatial extent to identify land degradation, to determine the cause(s) of the land degradation, and will enable remedies to be undertaken to reverse land degradation.

Data Source	Spatial Resolution(s)	Equatorial Temporal Frequency	Use	Analytical Approaches and Expected Outcomes
Landsat-8	30 m	3.7 days now with combined Sentinel-2a & Sentinel-2b data	Confirmation of land degradation from 2000 using Landsat-7 data to 2015 and beyond with Landsat-8 and -9 data.	30 m disaggregation of AVHRR and MODIS data to sub-national scales
Sentinel-2a & -2b	20 m	3.7 days now with combined Landsat-8; 3 days in 2020 when Landsat-9 joins the team	Confirmation of land degradation from 2016 and 2017 and into the 2020s.	Combined with Landsat data for 2016-2017 (data start in 2016). Combination of Landsat-8 and ESA Sentinel-2a and -2b observations will provide <4 day coverage for global land areas.
Commercial satellites	30 - 50 m	Coverage every 1-3 years	Local-scale confirmation of land degradation from 2010-2017 and beyond	Land degradation disaggregation to 30, 40, & 50 cm to understand drivers & processes at local level

Table 7. Sources of higher spatial resolution satellite data, their uses, and their analytical approaches and expected outcomes. The "harmonized" Landsat-8/Sentinel-2a/Sentinel-2b multi-spectral 30 m data have an equatorial revisit frequency of 3.7 days now. When Landsat-9 joins the team in 2020, the equatorial revisit frequency will drop to 3.0 days

We have organized our commercial satellite imagery into 100 x 100 km blocks at a 50 cm spatial resolution for both the panchromatic and our multi-spectral imagery. We are producing these mosaics now. These data will be invaluable for developing a highly-detailed mapping of land cover and land use for identifying land degradation and its drivers.

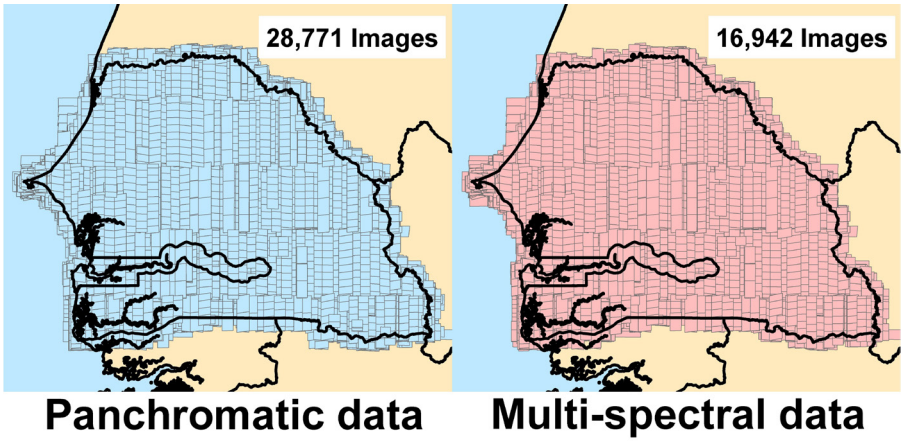

Figure 14. DigitalGlobe panchromatic and multi-spectral data for Senegal. All data are <20% cloud cover and available for our land degradation study. A comparable density of commercial satellite data is available for Uganda, Kenya, and Tanzania.

Mount Kenya. © Chris Murphy

X. CONCLUSIONS

X. CONCLUSIONS

We completed a wall-to-wall mapping effort based on satellite data and associated analyses to identify areas of potential land degradation at a 250 m resolution, through the combined use of NDVI, soil moisture, and precipitation data to identify areas of primary productivity decreases that are not related to climate. This mapping has been undertaken for Senegal, Uganda, Kenya, and Tanzania. In conjunction with this effort, we are producing a Landsat analysis in combination with wall-to-wall 50 cm commercial satellite data that enables identification of changes in land cover or land use and of fine-scale land degradation.

We have almost complete coverage of all four pilot countries at high resolution as we show for Senegal (Figure 14). Time series analyses based on these datasets in conjunction with data from moderate to high-resolution sensors such as 30 m Landsat, 30 m Aster, 20 m Sentinel-2a, and 30-50 cm commercial satellite data offer the potential to obtain the spatial and spectral detail necessary to interpret the drivers of observed changes in NDVI. A follow up report will demonstrate the usage of these datasets for setting baselines of land degradation in each of the four pilot countries.

Waste water from illegal gold mining operations in central Ghana. © Benjamin Drummond

XI. REFERENCES

XI. REFERENCES

Anav, A., et al. 2015. Spatiotemporal patterns of terrestrial gross primary production: *A review, Review of Geophysics* 53:785–818, doi:10.1002/2015RG000483.

Bai, Z. et al. 2008a. Proxy global assessment of land degradation. *Soil Use and Management* 24(3):223-234.

Bai, Z. et al. 2008b. Global Assessment of Land Degradation and Improvement: 1. Identification by Remote Sensing. GLADA Report Five, ISRIC World Soil Information and the Food and Agricultural Organization, 78 p.

Baldochi, D. et al. 2001. FLUXNET: a new tool to study the temporal and spatial variability of ecosystem-scale carbon dioxide, water vapor, and energy flux densities. *Bull. Am. meteorol.* Soc. 82(11): 2415–2434.

Balsamo, G. et al. 2015. ERA-Interim/Land: A global land surface reanalysis data set. *Hydrology Earth System Science* 19:389-407, doi:10.5194/hess-19-389-2015.

Beer, C. et al. 2010. Terrestrial gross carbon dioxide uptake: Global distribution and covariation with climate, Science 329:834–838.

Bentsen, M., et al. 2013. The Norwegian Earth System Model, NorESM1-M—Part 1: Description and basic evaluation of the physical climate, *Geosciences Model Development* 6:687–720.

Bierbaum, R. et al. 2014. Delivering global environmental benefits for sustainable development. Washington, D.C., Global Environment Facility.

Bormann, B. T. and G. E. Kiester 1979. *Pattern and Process in a Forested Ecosystem Sensing of Environment.* Springer-Verlag: New York.

Bosilovich, M. G. et al. 2015. MERRA-2: Initial Evaluation of the Climate. NASA Technical Report Series on Global Modeling and Data Assimilation. NASA/TM-2015- 104606, Vol. 43, NASA, GSFC Greenbelt, MD, USA, 139 pp. Available from http://gmao.gsfc.nasa.gov/pubs.

Brandt, M. et al. 2016. Woody plant cover estimation in drylands from Earth observation based seasonal metrics. *Remote Sensing of Environment* 172:28-38.

Clark, D. B., et al. 2011. The Joint UK Land Environment Simulator (JULES), model description—Part 2: Carbon fluxes and vegetation dynamics. *Geosciences Model Development* 4:701–722.

Collins, W. J., et al. 2011. Development and evaluation of an Earth-System model—HadGEM2. *Geosciences Model Development* 4:1051–1075.

Deering, D. W. 1978. Rangeland reflectance characteristics measured by aircraft and spacecraft sensors. Ph.D. dissertation Teaxas A&M University, College Station, 338 pp.

Dufresne, J.-L., et al. 2013. Climate change projections using the IPSL-CM5 Earth system model: From CMIP3 to CMIP5. *Climate Dynamics* 40:2123–2165.

Evans, J. and Geerken, R., 2004. Discrimination between climate and human-induced dryland degradation. *Journal Arid Environ.* 57: 535-554.

Fan, Y. and van den Dool, H., 2004. Climate prediction center global monthly soil moisture data set at 0.5o resolution for 1948 to present. *Journal of Geophysical Research* 109: D10102.

Fensholt, R. et al. 2006. Evaluating MODIS, MERIS, and SPOT-Veg vegetation indices using in situ measurements in a semiarid environment. IEEE-TGARS 44(7):1774-1786.

Fensholt, R. and Rasmussen, K. 2011. Analysis of trends in the Sahelian 'rain-use efficiency' using GIMMS NDVI, RFE and GPCP rainfall data. *Remote Sensing of Environment*, 115:438-451.

Fensholt, R. and Proud, S. R. 2012. Evaluation of Earth Observation based global long-term vegetation trends — Comparing GIMMS and MODIS global NDVI time series. *Remote Sensing of Environment*, 119:131-147.

Fensholt, R. et al. 2013. Assessing Land Degradation/Recovery in the African Sahel from long-term Earth observation based primary productivity and precipitation relationships. *Remote Sensing*, 5, 664-686.

Frankenberg, C et al. 2011. New global observations of the terrestrial carbon cycle from GOSAT: Patterns of plant fluorescence with gross primary productivity, *Geophysical Research Letters* 38, L17706, doi:10.1029/2011GL048738.

Gardner, W. R. 1983. Soil moisture properties and efficient water use: An Overview. Pages 45-64 in Limitations to Efficient Water Use in Crop Production. H. M. Taylor, W.R. Jordan, and T.R. Sinclair, editors. *American Society of Agronomy*, Madison.

GEF, 2015. Sustainable Land Management Financing in the GEF, A Primer for the Sixth GEF Replenishment Phase (GEF-6). Global Environmental Facility, Washington, DC. Accessed 5-1-2015. http://www.thegef.org/sites/default/files/publications/GEF_LDFAbrochure_CRA_2_0_0.pdf.

Gent, P. R., et al. 2011. The Community Climate System Model version 4. *Journal of Climate,* 24:4973–4991.

Goulas, Y. A et al. 2017. Gross primary production of a wheat canopy relates stronger to far red than to red solar-induced chlorophyll fluorescence. *Remote Sensing* 9, 97; doi:10.3390/rs9010097.

Guanter, L. et al. 2014. Global and time-resolved monitoring of crop photosynthesis with chlorophyll fluorescence, *Proceedings of the National Academy of Science U.S.A.* 111(E1):327–333.

Hein, L. and De Ridder, N., 2006. Desertification in the Sahel: A reinterpretation. Global Change. Bio., 12, 751-758.

Hein, L. et al. 2011. Desertification in the Sahel: Towards better accounting for ecosystem dynamics in the interpretation of remote sensing images. *J. Arid Environ.*, 75, 1164-1172

Herrmann, S. M., et al. 2014. People and pixels in the Sahel: A study linking coarse-resolution remote sensing observations to land users' perceptions of their changing environment in Senegal. *Ecol. Soc*, 19.

Herrmann, S. M., Tappan, G. G. 2013. Vegetation impoverishment despite greening: A case study from central Senegal. *Journal of Arid Environ.*, 90: 55-56.

Higginbottom, T. P. and Symeonakis, E., 2014. Assessing Land Degradation and Desertification Using Vegetation Index Data: Current Frameworks and Future Directions. *Remote Sensing*, 6(10), 9552-9575.

Huete, A., et al. 2002. Overview of the radiometric and biophysical performance of the MODIS vegetation indices. *Remote Sensing of Environment* 83:195-213.

Ibrahim, Y. et al. 2015. Land degradation assessment using residual trend analysis of GIMMS NDVI3g, soil moisture and rainfall in sub-Saharan West Africa from 1982 to 2012. *Remote Sensing* 7: 5471-5494.

Joiner, J. et al. 2011. First observations of global and seasonal terrestrial chlorophyll fluorescence from space, *Biogeosciences* 8:637–651.

Joiner, J. et al. 2014. The seasonal cycle of satellite chlorophyll fluorescence observations and its relationship to vegetation phenology and ecosystem atmosphere carbon exchange. *Remote Sensing of Environment* 152:375-391.

Jiang, Z., et al. 2008. Development of a two-band enhanced vegetation index without a blue band. *Remote Sensing of Environment* 112:3833-3845.

Jung, M. et al. 2011. Global patterns of land-atmosphere fluxes of carbon dioxide, latent heat, and sensible heat derived from eddy covariance, satellite, and meteorological observations. Journal of Geophysical Research 116, G00J07, doi:10.1029/2010JG001566.

Krinner, G., N. et al. 2005. A dynamic global vegetation model for studies of the coupled atmosphere-biosphere system. *Global Biogeochemical Cycles* 19:GB1015, doi:10.1029/2003GB002199.

Mandanici, E. and G. Bitelli 2016. Preliminary comparison of Sentinel-2 and Landsat-8 Imagery for a combined use. *Remote Sensing* 8:1014-1024.

Masek, J. et al. 2016. Harmonizing Landsat and Sentinel-2 reflectances for better land monitoring. NASA GSFC *Hydrospheric and Biospheric Science*. http://hls.gsfc.nasa.gov/ and https://nex.nasa.gov/nex/projects/1371 accessed on January 20, 2017.

Maxwell, K. and G. N. Johnson 2000. Chlorophyll fluorescence—a practical guide. *Journal of Experimental Botany* 51(354):659-668.

Myneni, R.B. et al. 1995. The interpretation of spectral vegetation indexes. *IEEE Transactions on Geoscience and Remote Sensing* 33:481–486.

Oldeman, L. et al. 1990. World map on status of human-induced soil degradation (GLASOD) UNEP. ISRIC, Nairobi, Kenya.

Oleson, K. W. et al. 2010. Technical description of version 4.0 of the Community Land Model (CLM). NCAR Technical Note NCAR/TN-478+STR,doi:10.5065/D6FB50WZ.

Pinzon, J. E. and Tucker C. 2014. A non-stationary 1981-2012 AVHRR NDVI3g time series. *Remote Sensing*, doi:10.3390/rs50x000x, July 2014.

Prince, S. D. et al. 2007. Desertification in the Sahel: A reinterpretation of a reinterpretation. *Global Change Bio*., 13:1308-1313.

Reichle, R. et al. 2016. Assessment of MERRA-2 land surface hydrology estimates. *Journal of Climate*. doi:10.1175/JCLI-D-16-0720.1, in press.

Rouse, J. W. et al. 1974. Monitoring vegetation systems in the Great Plains with ERTS. *Proceedings, third Earth Resource Technology Satellite (ERTS) Symposium,* NASA SP-351: 309-317.

Sellers, P. J. 1985. Canopy reflectance, photosynthesis, and transpiration. *International Journal of Remote Sensing* 6(8):1335-1372.

Sellers, P. J. 1987. Canopy reflectance, photosynthesis, and transpiration II: The role of biophysics in the linearity of their interdependence. *Remote Sensing of Environment* 21:143-183.

Sellers, P. J. et al. 1997. Modeling the Exchanges of Energy, Water, and Carbon between Continents and the Atmosphere. *Science* 275:502-509.

Sedano, F. et al. 2016. The impact of charcoal production on forest degradation: a case study in Tete, Mozambique. *Environmental Research Letters* 11:094020, doi:10.1088/1748-9326/11/9/094020

Sitch, S. et al. 2015. Recent trends and drivers of regional sources and sinks of carbon dioxide. Biogeosciences 12:653–679.

Taylor, K. E. et al. 2012. An overview of CMIP5 and the experiment design, *Bulletin American Meteorological Society* 90:485–498, doi:10.1175/BAMS-D-11-00094.1.

Tucker, C.J. 1979. Red and photographic infrared linear combinations for monitoring vegetation. *Remote Sensing of Environment* 8:127–150.

Turner, D. P. 2006. Evaluation of MODIS NPP and GPP products across multiple biomes. *Remote Sensing of Environment* 102:282–292.

UN. 2016. Sustainable Development Goals: Goal 15 Protect, restore and promote sustainable use of terrestrial ecosystems, sustainably manage forests, combat desertification, and halt and reverse land degradation and halt biodiversity loss. https://unstats.un.org/sdgs/files/metadata-compilation/Metadata-Goal-15.pdf

UNCCD. 2013. Report of the Conference of the Parties on its eleventh session, held in Windhoek from 16 to 27 September 2013. United Nations Convention to Combat Desertification. Accessed 3-8-2017. http://www.unccd.int/Lists/OfficialDocuments/cop11/23add1eng.pdf

UNEP, Middleton, N. and Thomas, D.S.G, 1997. World atlas of desertification London. United Nations.

van den Dool et al. 2003. Performance and analysis of the constructed analogue method applied to U.S. soil moisture over 1981–2001. *Journal of Geophysics and Research Atmospheres* 108, 8617. doi:10.1029/2002JD003114

Vargas, M. et al. 2013. An initial assessment of Suomi NPP VIIRS vegetation index EDR. *Journal of Geophysical Research: Atmospheres* 118, 1-16. doi:10.1002/2013JD020439JD003114

Vincent, J. et al. 2016. FLEX end-to-end mission performance simulation. *IEEE Transactions on Geoscience and Remote Sensing* 54(7):4215-4223.

Wei, Y. et al. 2014. The North American Carbon Program multi-scale synthesis and terrestrial model inter-comparison project—Part 2: Environmental driver data. *Geoscience Model Development Discussions* 6:5375–5422.

Wessels, K. J. et al. 2004. Assessing the effects of human-induced land degradation in the former homelands of northern South Africa with a 1 km AVHRR NDVI. *Remote Sen. Environ*. 91:47-67.

Wessels, K. J. et al. 2007. Can human-induced land degradation bi distinguished from the effects of rainfall variability? A case study in South Africa. *J. Arid Environ*. 68:271-297.

Wessels, K. J. et al. 2012. Limits to detectability of land degradation by trend analysis of vegetation index data. *Remote Sen. Environ*. 125:10-22.

Wood, J. D. et al. 2017. Multi-scale analyses of solar-induced florescence and gross primary production. *Geophysical Research Letters* 44:533–541, doi:10.1002/2016GL070775.

Yengoh, G.T. et al. 2014. The use of the Normalized Difference Vegetation Index (NDVI) to assess land degradation at multiple scales: a review of the current status, future trends, and practical considerations. *Springer Briefs in Environmental Science, Springer International Publishing*, 110 p.

Yokota, T. et al. 2009. Global concentrations of CO2 and CH4 retrieved from GOSAT: First preliminary results. *Sola* 5:160-163, doi10.2151/sola.20090-041.

Yoshida, Y. et al. 2015. The 2010 Russian drought impact on satellite measurements of solar-induced chlorophyll fluorescence: Insights from modeling and comparisons with parameters derived from satellite reflectances. *Remote Sensing of Environment* 166:163-177.

Zhang, Y. et al. 2016. Consistency between sun-induced chlorophyll fluorescence and gross primary production of vegetation in North America. *Remote Sensing of Environment* 183:154–169.

Zhao, M. et al. 2005. Improvements of the MODIS terrestrial gross and net primary production global data set. *Remote Sensing of Environment* 95:164–176.

Zhao, M., and S. W. Running. 2010. Drought-induced reduction in global terrestrial net primary production from 2000 through 2009. *Science* 329:940–943.

XII. APPENDIX

XII. APPENDIX

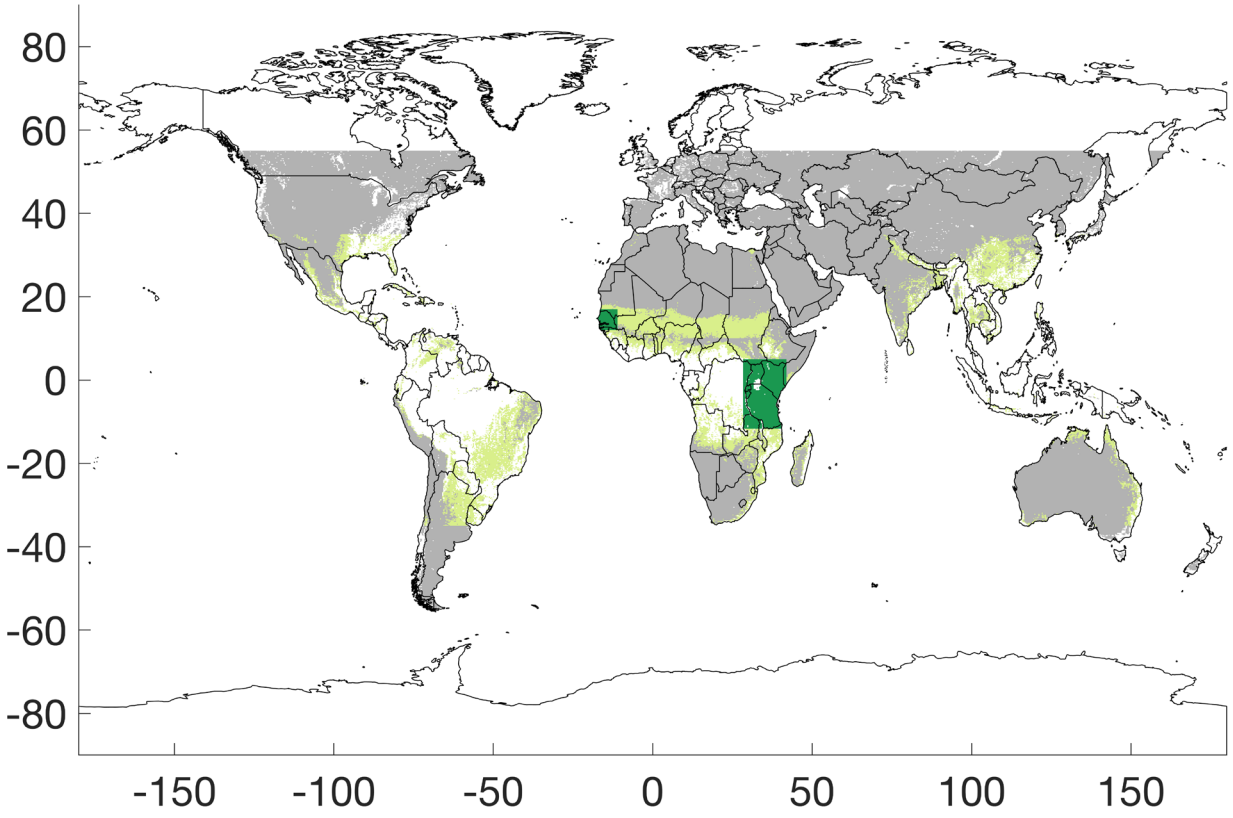

Figure A.1. The four pilot countries (Senegal, Kenya, Uganda and Tanzania, in dark green) and the world humidity classes from tropical Dry-sub-humid, and semi-arid classes in the Sahel (light green). The Dry-sub-humid class is computed empirically as NDVI long-term average in the range 0.6<NDVI<0.75). The empirical humidity classes well match the classes defined in the "world atlas of desertification" (UNEP, 1997). We select randomly about 4 million points distributed as 90% within the four countries (about 10% points within the region) and 10% from other areas in the Sahel that are tropical dry-sub-humid or semi-arid (about 1% within these classes).

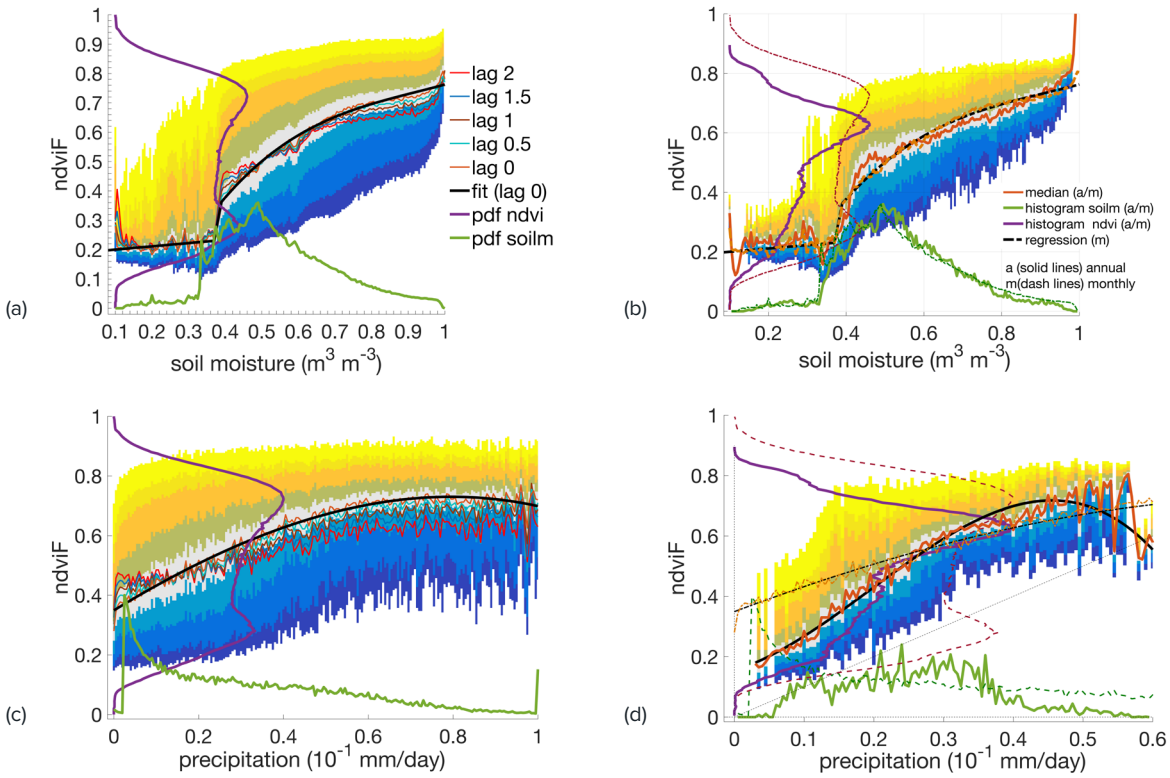

Figure A.2. (a) Global relationship between soil moisture and NDVI at different time lags (0-4 bi-monthly periods), (b) comparison between annual integrated soil moisture and NDVI. (c) Global relationship between precipitation and NDVI at different time lags (0-4), and (d.) comparison between annual integrated precipitation and NDVI. Data for this figure are derived from NDVI3g, GPCP and MERRA-2 data from 1982 – 2015 using 9 million random points for the lags (a, c) and 1 million for the annual (b,d). The time lags for the NDVI3g data are bi-monthly composite periods. Composites are formed from day 1 to day 15 of every month and from day 16 to the end of the month.

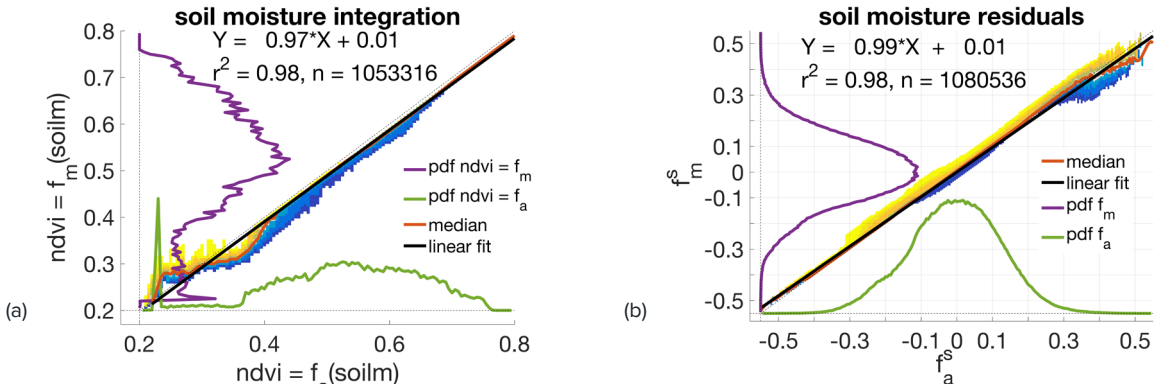

Figure A.3. a) Comparison of the integrals of predicted NDVI using soil moisture at monthly (fm(soil)) and annual integrals (fa(soil)). The consistency of the functional is apparent in the one to one relationship between fm(soil) and fa(soil) even though they generate different probability density functions (green and purple lines). As expected, the predicted NDVI from annual integrals by fa(soil) (x-axis) is smoother than the predictions from monthly soil data (fm(soil)) (y-axis), and the functional appears invariant. b) Comparison of the residuals of NDVI using soil moisture at monthly (f sm) and annual levels (f sa). The Gaussian-tendency of the probability density functions shows that vegetation variability is dominated and captured by the soil moisture as a climate variable.

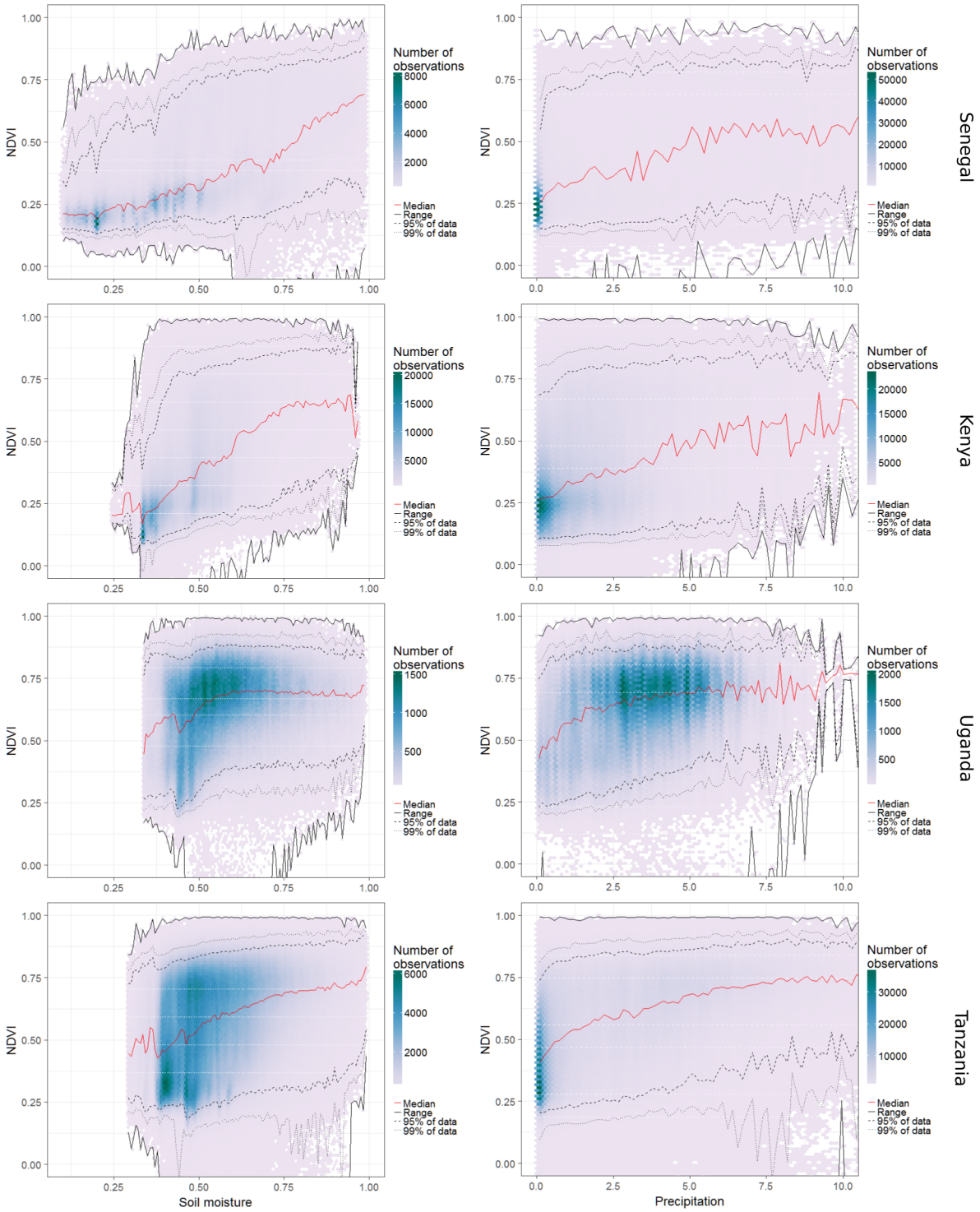

Figure A.4. Relationship between soil moisture and NDVI, and between precipitation and NDVI, for each of the four pilot countries. Data for this figure are derived from NDVI3g, GPCP, and MERRA-2 data from 1982 – 2015.

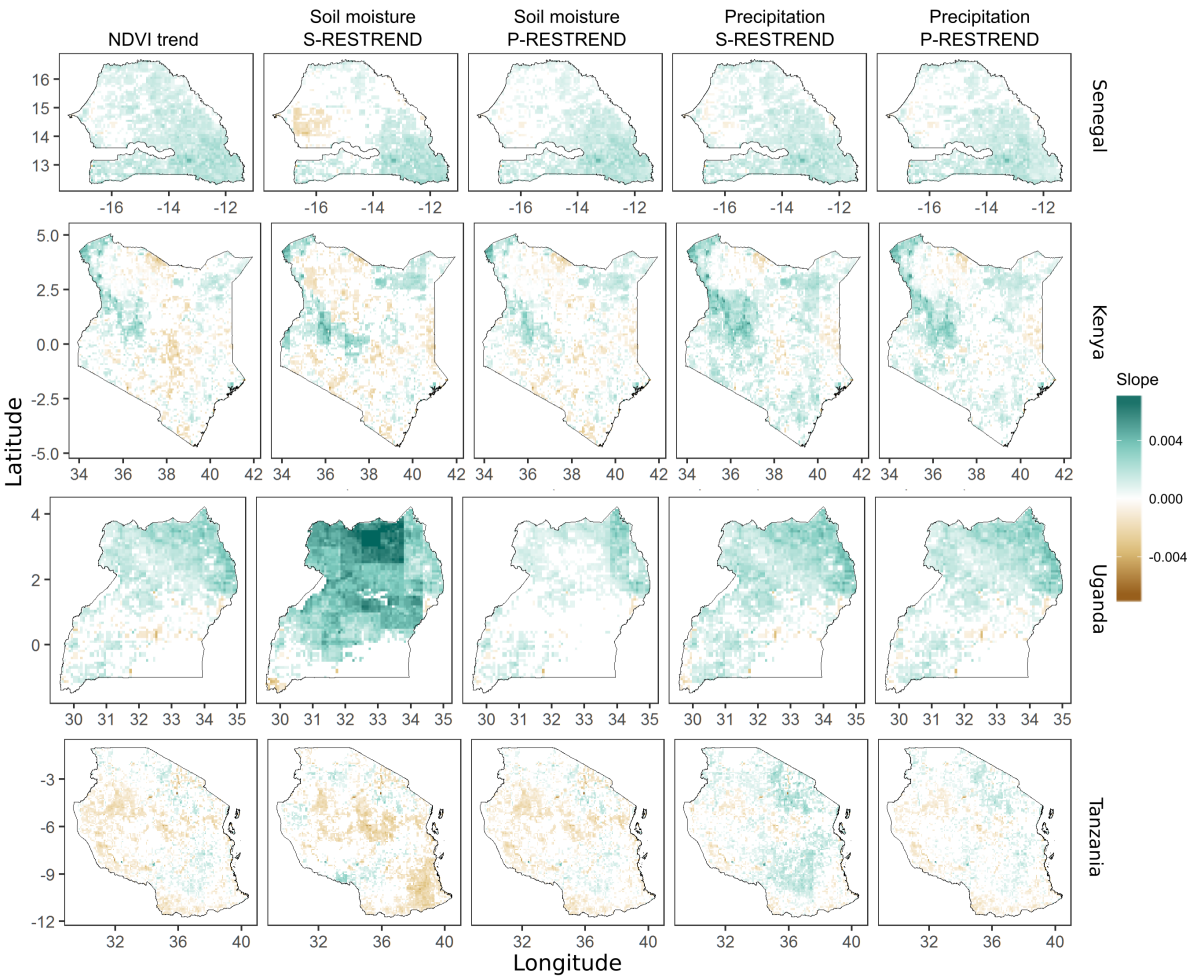

Figure A.5. Comparison of alternative methods for removing climate effects from the vegetation index signal. P-RESTREND indicates the pointwise RESTREND approach, and S-RESTREND indicates the system RESTREND approach. The maps that refer to soil moisture use the MERRA-2 dataset. The maps that refer to precipitation use the GPCP dataset. All the maps in this figure use AVHRR NDVI3g data. The trends were calculated over 1982-2015 for each of the four countries.. Only trends significant at the $p < 0.05$ level (using a Mann-Kendall test) are shown.

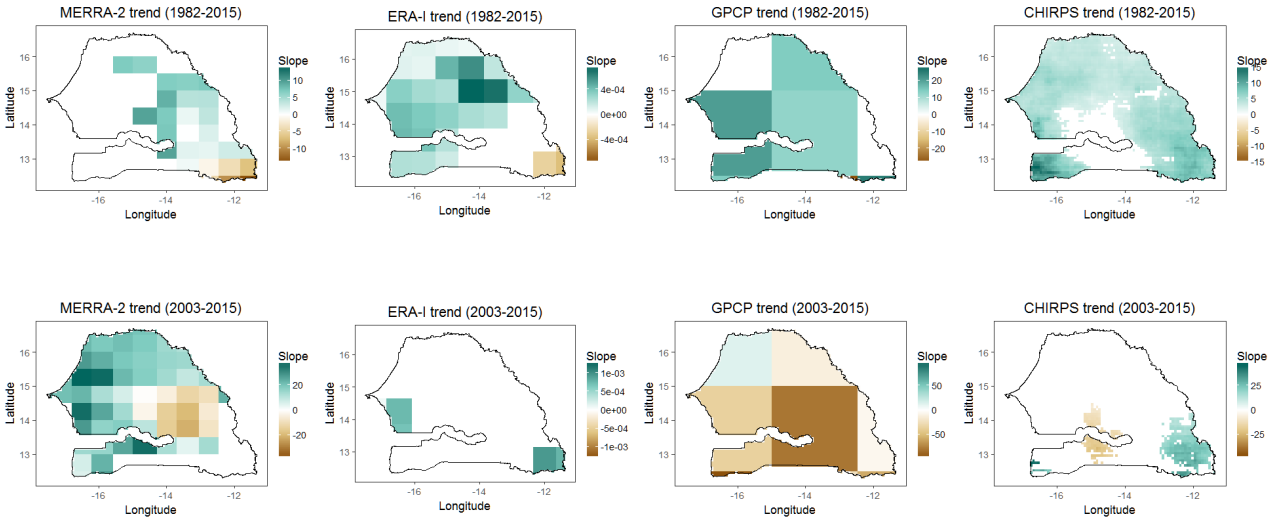

Figure A.6. Trends of mean annual soil moisture (MERRA-2 and ERA-I), and total annual precipitation (GPCP and CHIRPS) in Senegal over the periods of the AVHRR3g (1982-2015 top panel) and MODIS (2003-2015 bottom panel) data used in this study. Only trends significant at the $p < 0.05$ level (using a Mann-Kendall test) are shown.

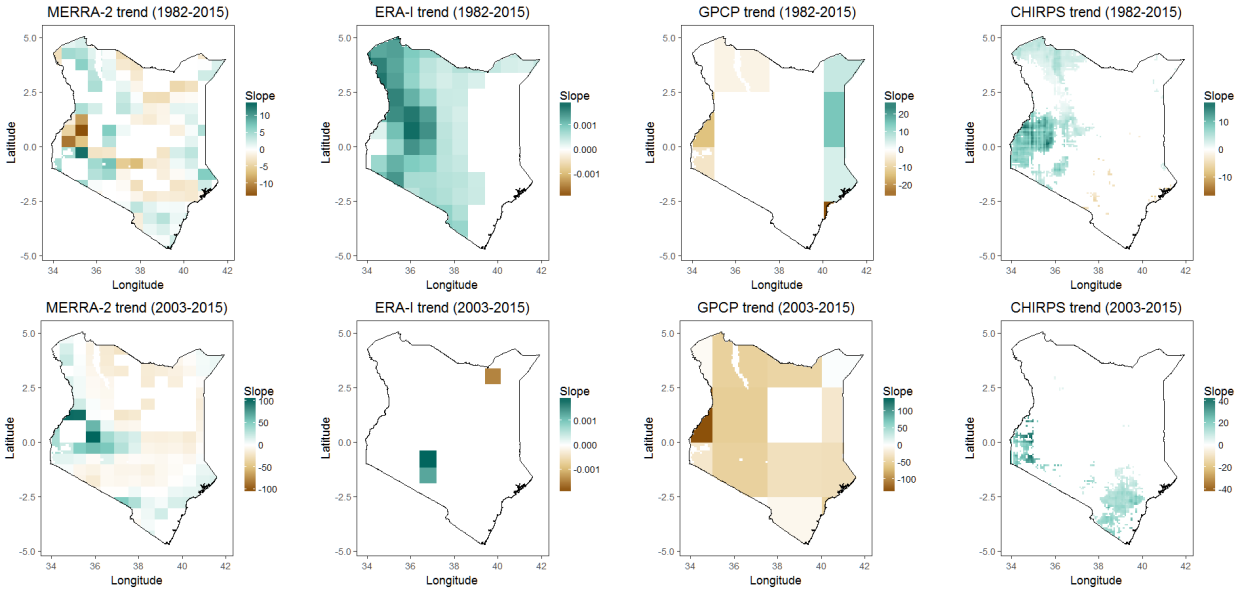

Figure A.7. Trends of mean annual soil moisture (MERRA-2 and ERA-I), and total annual precipitation (GPCP and CHIRPS) in Kenya over the periods of the AVHRR3g (1982-2015 top panel) and MODIS (2003-2015 bottom panel) data used in this study. Only trends significant at the $p < 0.05$ level (using a Mann-Kendall test) are shown.

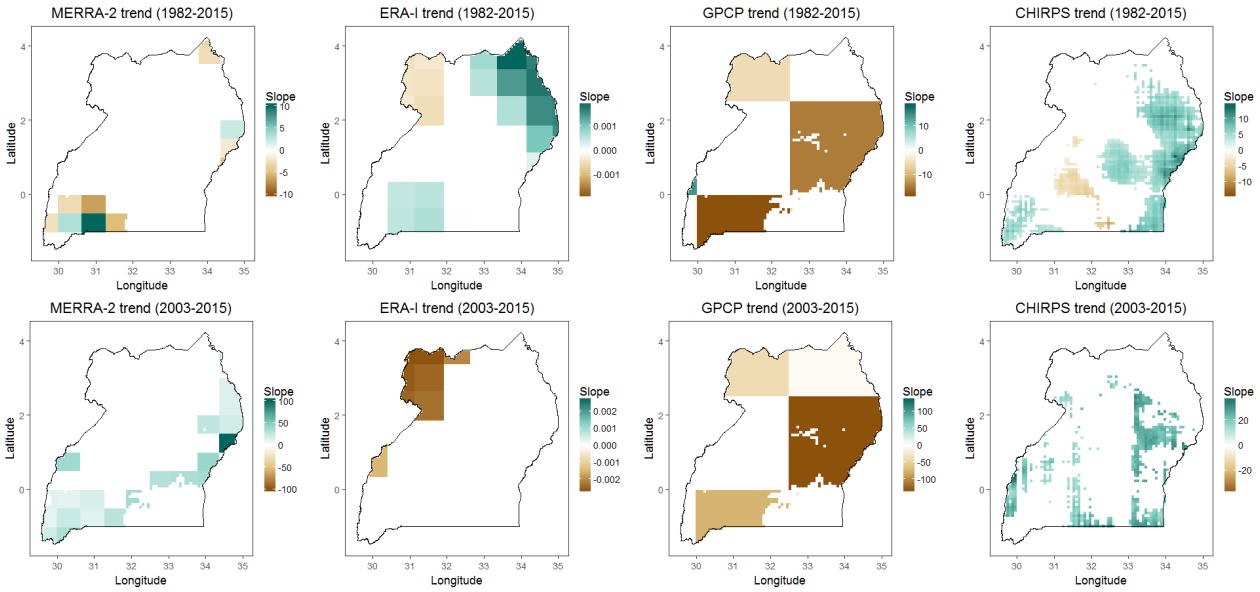

Figure A.8. Trends of mean annual soil moisture (MERRA-2 and ERA-I), and total annual precipitation (GPCP and CHIRPS) in Uganda over the periods of the AVHRR3g (1982-2015 top panel) and MODIS (2003-2015 bottom panel) data used in this study. Only trends significant at the $p < 0.05$ level (using a Mann-Kendall test) are shown.

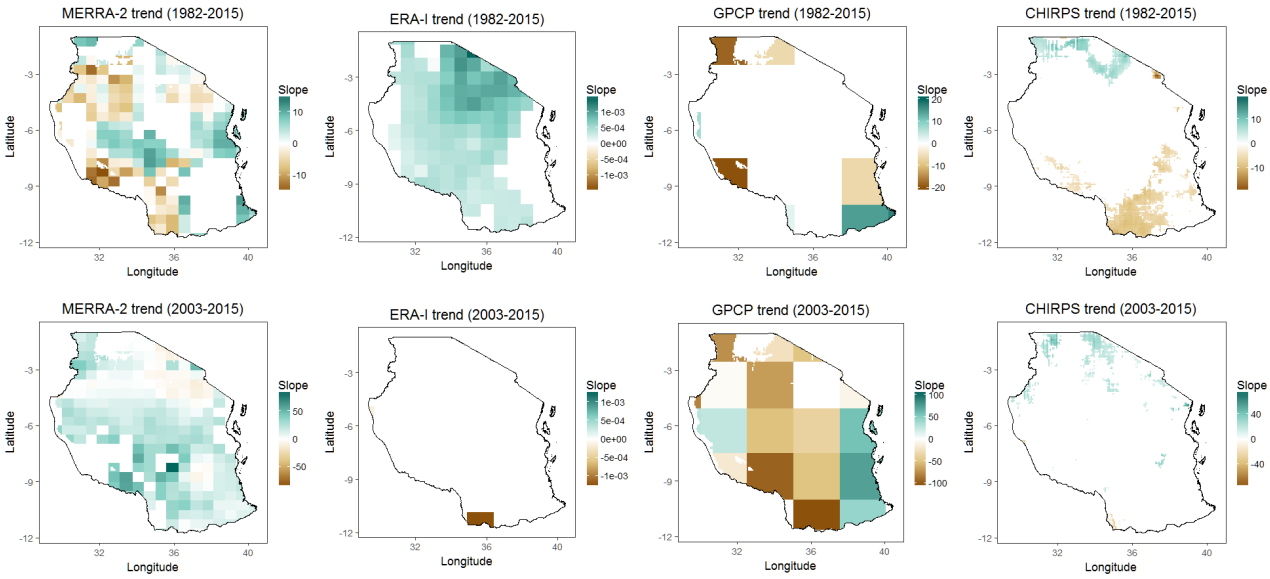

Figure A.9. Trends of mean annual soil moisture (MERRA-2 and ERA-I), and total annual precipitation (GPCP and CHIRPS) in Tanzania over the periods of the AVHRR3g (1982-2015 top panel) and MODIS (2003-2015 bottom panel) data used in this study. Only trends significant at the $p < 0.05$ level (using a Mann-Kendall test) are shown.

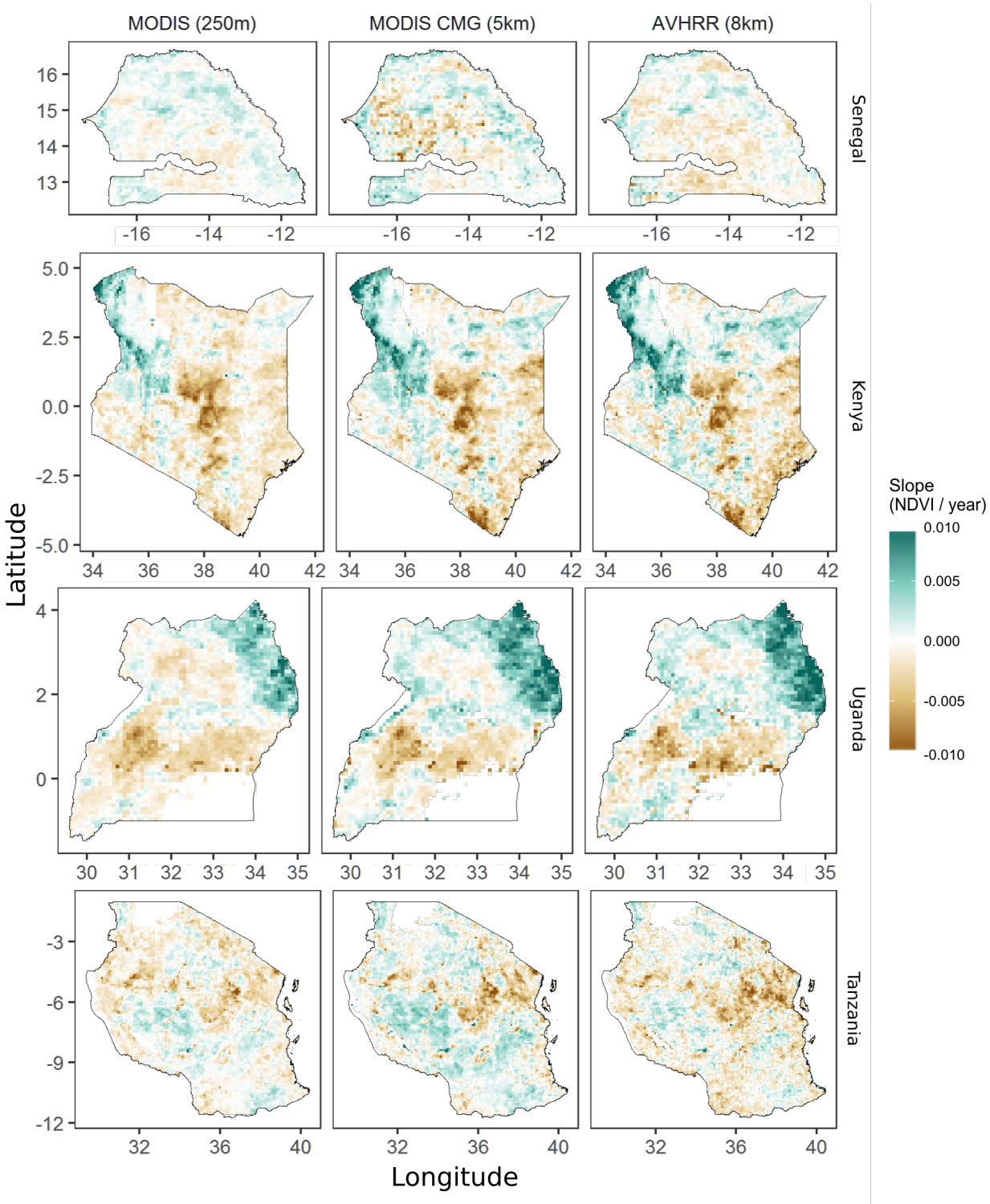

Figure A.10. Comparison of growing season integrals of NDVI trends by sensor and by dataset for each of the four pilot countries. All data are mapped after aggregation (250 m MODIS, using mean value) or nearest neighbor resampling (5 km MODIS CMG) to an eight-km resolution for the 2003-2015 time period. The growing season dates used in the integration were calculated from the full 1982-2015 AVHRR NDVI3g NDVI record.

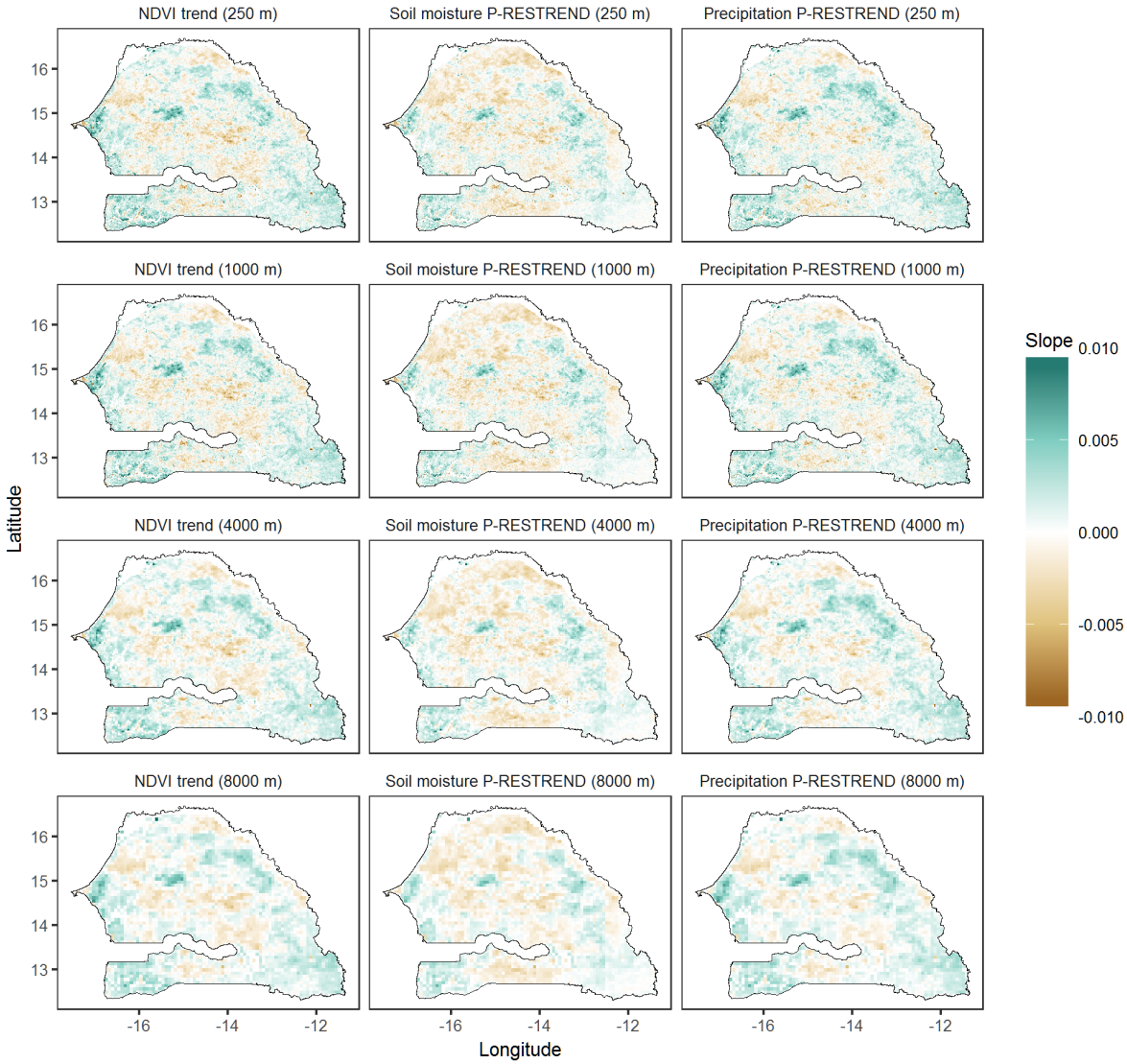

Figure A.11. Senegal NDVI trend and pointwise RESTREND results when scaling data from 250 m to 8 km resolution. All results based on MODIS MOD13Q1 data from 2003-2015. Only trends significant at the $p < 0.05$ level (using a Mann-Kendall test) are shown.

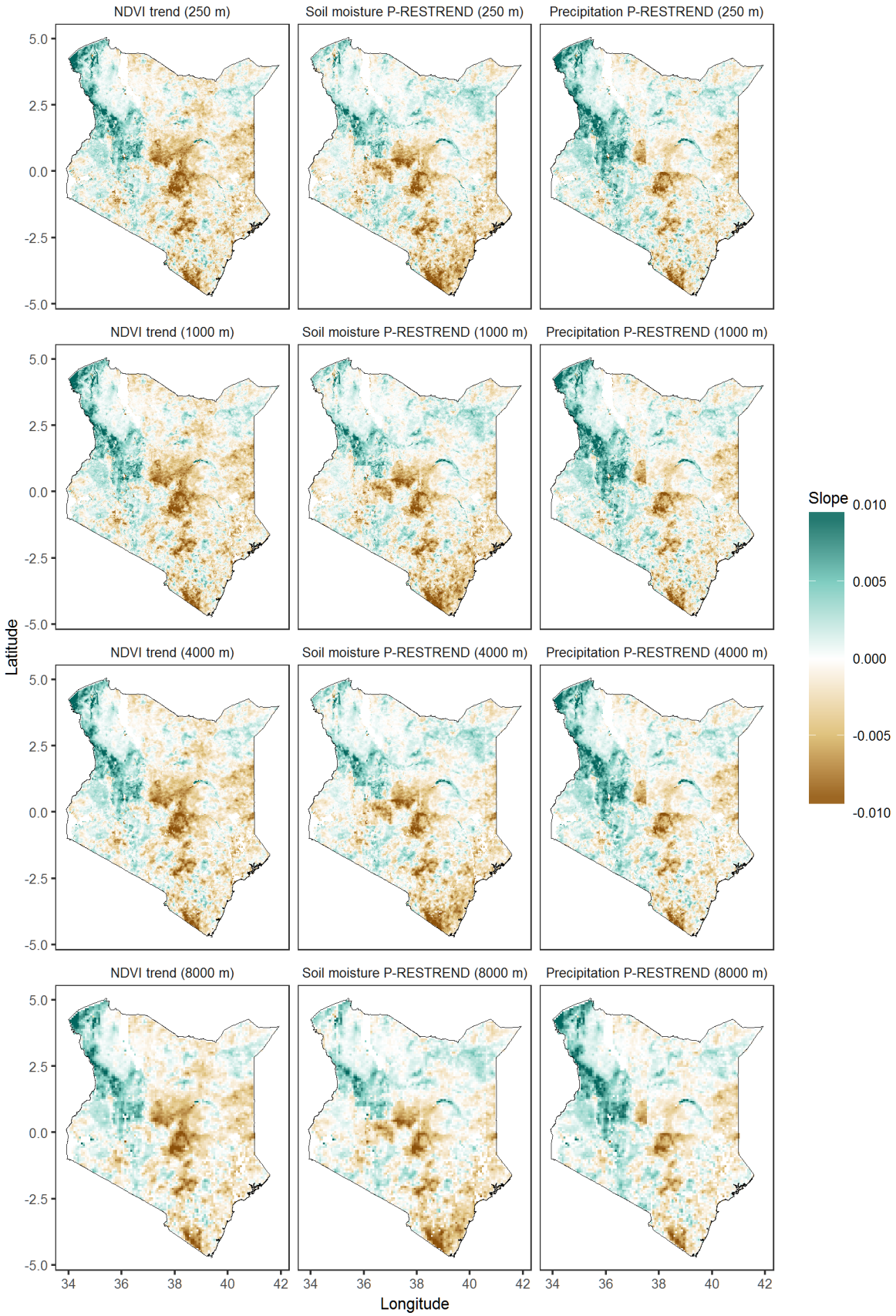

Figure A.12. Kenyan NDVI trend and pointwise RESTREND results when scaling data from 250 m to 8 km resolution. All results based on MODIS MOD13Q1 data from 2003-2015. Only trends significant at the $p < 0.05$ level (using a Mann-Kendall test) are shown.

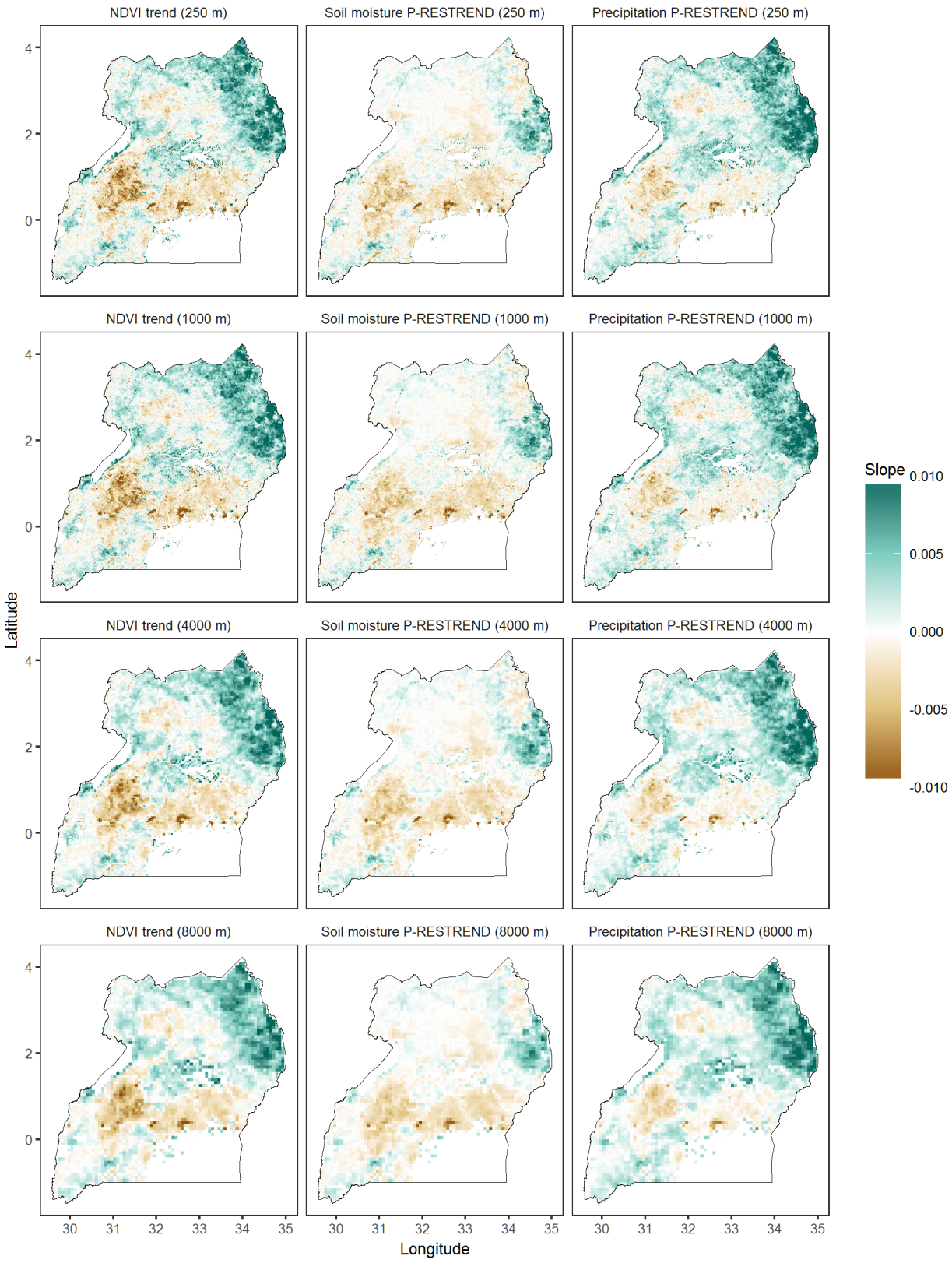

Figure A.13. Uganda NDVI trend and pointwise RESTREND results when scaling data from 250 m to 8 km resolution. All results based on MODIS MOD13Q1 data from 2003-2015. Only trends significant at the $p < 0.05$ level (using a Mann-Kendall test) are shown.

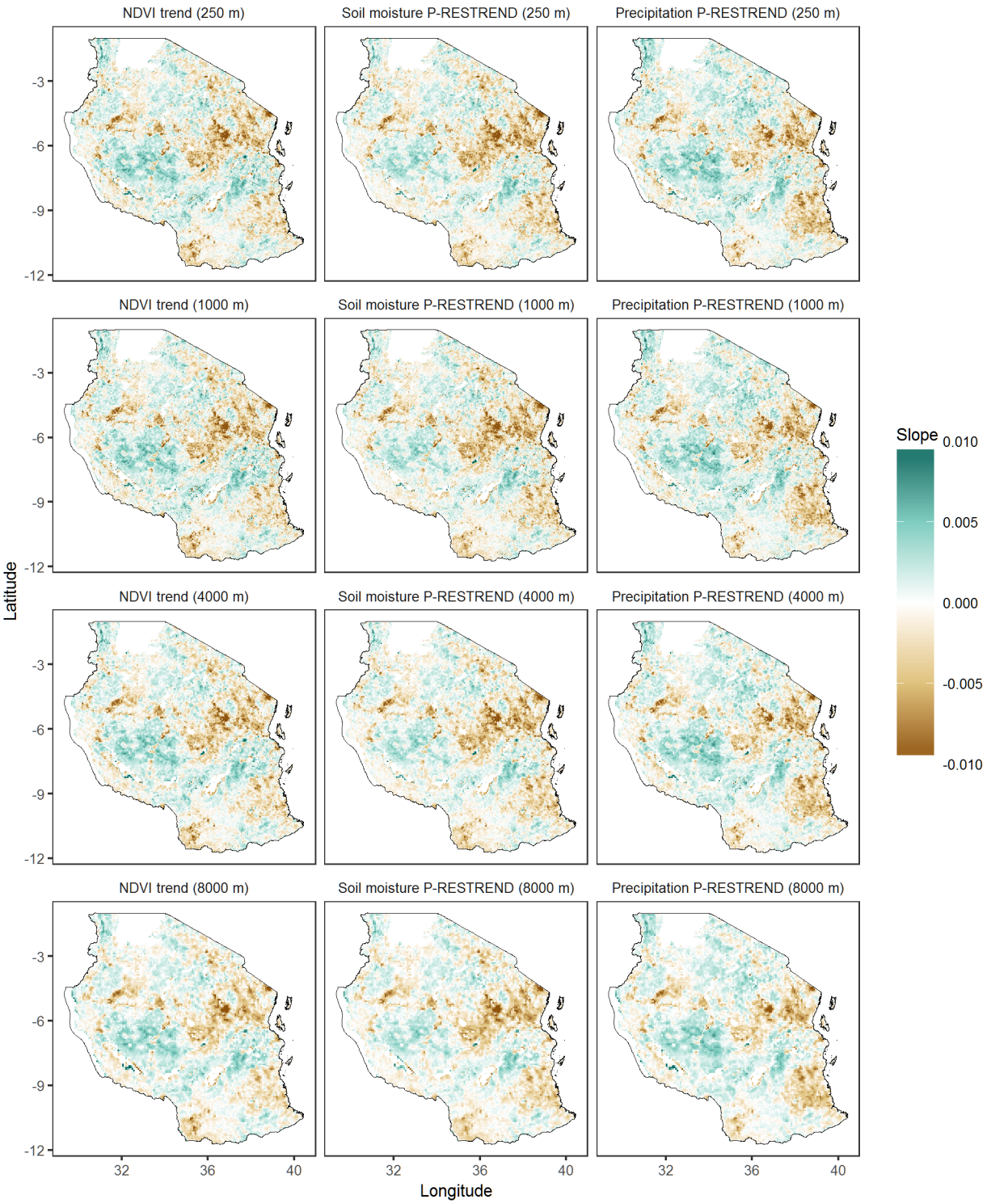

Figure A.14. Tanzania NDVI trend and pointwise RESTREND results when scaling data from 250 m to 8 km resolution. All results based on MODIS MOD13Q1 data from 2003-2015. Only trends significant at the $p < 0.05$ level (using a Mann-Kendall test) are shown.

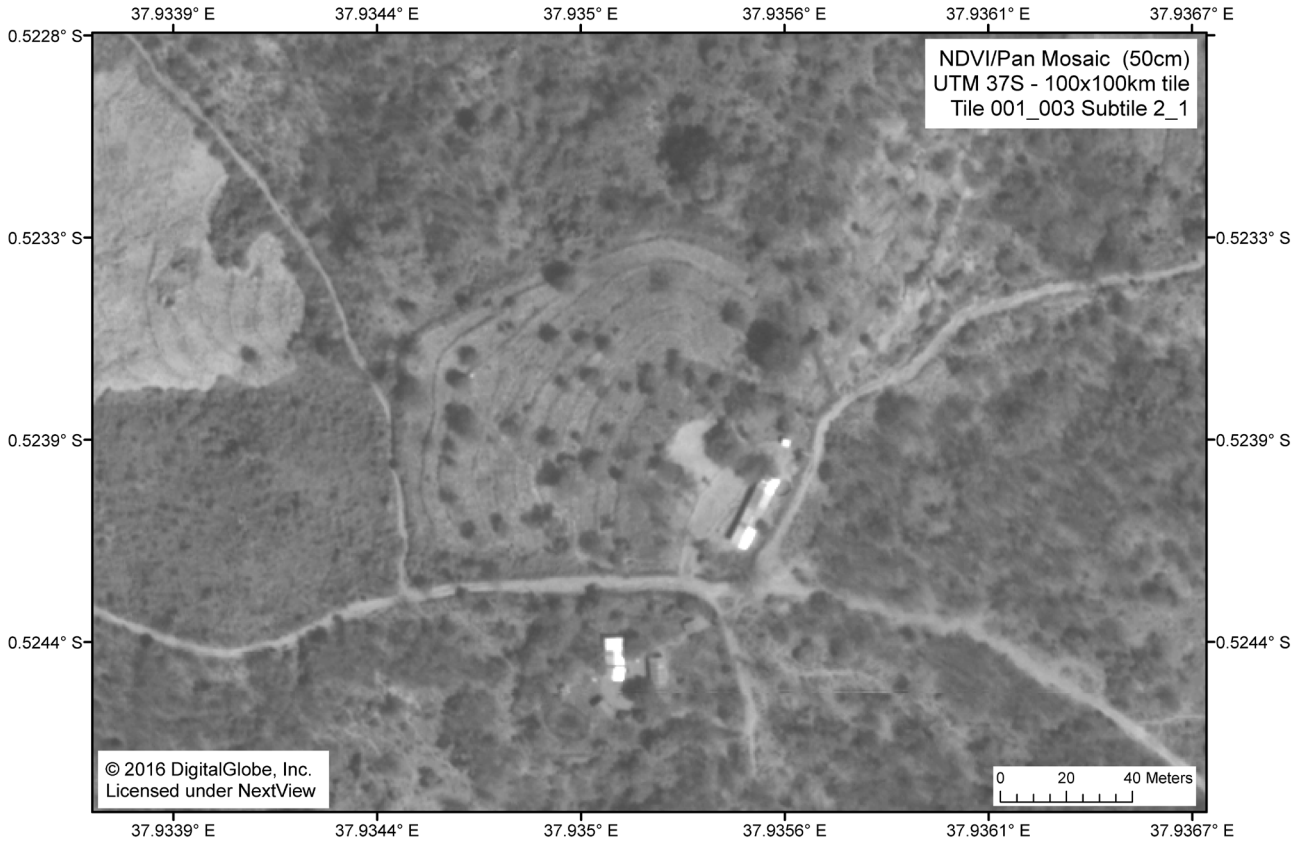

Figure A. 15. An example of a 50 cm commercial satellite data mosaic for one of the areas in Kenya where we decreases in primary productivity in Figure 9.

CONSERVATION INTERNATIONAL

gef
GLOBAL ENVIRONMENT FACILITY
INVESTING IN OUR PLANET

LUND UNIVERSITY

NASA